Cell

A Chromatin-Dependent Role of the Fragile X Mental Retardation Protein FMRP in the DNA Damage Response

Roman Alpatov,[1,2,11] Bluma J. Lesch,[3,11] Mika Nakamoto-Kinoshita,[4] Andres Blanco,[1,2] Shuzhen Chen,[1,2] Alexandra Stützer,[5] Karim J. Armache,[6] Matthew D. Simon,[6] Chao Xu,[7] Muzaffar Ali,[8] Jernej Murn,[1,2] Sladjana Prisic,[9] Tatiana G. Kutateladze,[8] Christopher R. Vakoc,[10] Jinrong Min,[7] Robert E. Kingston,[6] Wolfgang Fischle,[5] Stephen T. Warren,[4] David C. Page,[3] and Yang Shi[1,2,*]

[1]Division of Newborn Medicine, Boston Children's Hospital, Boston, MA 02115, USA
[2]Department of Cell Biology, Harvard Medical School, Boston, MA 02115, USA
[3]Howard Hughes Medical Institute, Whitehead Institute and Department of Biology, Massachusetts Institute of Technology, Cambridge, MA 02142, USA
[4]Departments of Human Genetics, Biochemistry, and Pediatrics, Emory University School of Medicine, Atlanta, GA 30322, USA
[5]Laboratory of Chromatin Biochemistry, Max Planck Institute for Biophysical Chemistry, 37077 Göttingen, Germany
[6]Massachusetts General Hospital, Department of Molecular Biology and Department of Genetics, Harvard Medical School, Boston, MA 02114, USA
[7]Structural Genomics Consortium and Department of Physiology, University of Toronto, Toronto ON M5G 1L7, Canada
[8]Department of Pharmacology, University of Colorado School of Medicine, Aurora, CO 80045, USA
[9]Division of Infectious Diseases, Boston Children's Hospital and Harvard Medical School, Boston, MA 02115, USA
[10]Cold Spring Harbor Laboratory, Cold Spring Harbor, NY 11724, USA
[11]Co-first authors
*Correspondence: yang_shi@hms.harvard.edu
http://dx.doi.org/10.1016/j.cell.2014.03.040

SUMMARY

Fragile X syndrome, a common form of inherited intellectual disability, is caused by loss of the fragile X mental retardation protein FMRP. FMRP is present predominantly in the cytoplasm, where it regulates translation of proteins that are important for synaptic function. We identify FMRP as a chromatin-binding protein that functions in the DNA damage response (DDR). Specifically, we show that FMRP binds chromatin through its tandem Tudor (Agenet) domain in vitro and associates with chromatin in vivo. We also demonstrate that FMRP participates in the DDR in a chromatin-binding-dependent manner. The DDR machinery is known to play important roles in developmental processes such as gametogenesis. We show that FMRP occupies meiotic chromosomes and regulates the dynamics of the DDR machinery during mouse spermatogenesis. These findings suggest that nuclear FMRP regulates genomic stability at the chromatin interface and may impact gametogenesis and some developmental aspects of fragile X syndrome.

INTRODUCTION

Chromatin is a complex biological entity comprised of DNA wrapped around histone octamers (Wolffe and Guschin, 2000). Posttranslational modifications of histone proteins serve as an interface for various chromatin "readers," which are chromatin-binding proteins that coordinate downstream processes, including the DNA damage response (DDR) and repair events (Costelloe et al., 2006; Downs et al., 2007; Stucki and Jackson, 2006). The mammalian DDR pathway is initiated by the activation of several conserved protein kinases, including ATM and ATR, which are members of the phosphatidylinositol 3-kinase-related kinase (PIKK) family. While ATM is activated by DNA double-strand breaks (DSBs), ATR activity is triggered by stalled replication forks as well as single-strand DNA (Ciccia and Elledge, 2010). Upon activation, ATR phosphorylates histone H2A.X at serine 139 (termed γH2A.X) (Ciccia and Elledge, 2010; Liu et al., 2006; Ward and Chen, 2001) and the breast cancer-associated tumor-suppressor protein BRCA1 at serine 1423 (Gatei et al., 2001; Tibbetts et al., 2000). Both γH2A.X and BRCA1 are important regulators of genomic stability (Celeste et al., 2002; Nagaraju and Scully, 2007).

The fragile X mental retardation protein FMRP is an RNA-binding protein that functions mainly at the neuronal dendrites, where it associates with specific mRNAs and modulates their translation, thus regulating a subset of proteins involved in synaptic function (Bassell and Warren, 2008; Brown et al., 2001). FMRP is critical for metabotropic glutamate receptor (mGluR)-dependent long-term depression, as well as other forms of synaptic plasticity. The lack of FMRP due to *FMR1* gene silencing results in fragile X syndrome, a common form of inherited intellectual disability and one of the leading causes of autism (Bear et al., 2004; Garber et al., 2008; Nelson, 1995; O'Donnell and Warren, 2002; Santoro et al., 2012; Warren and

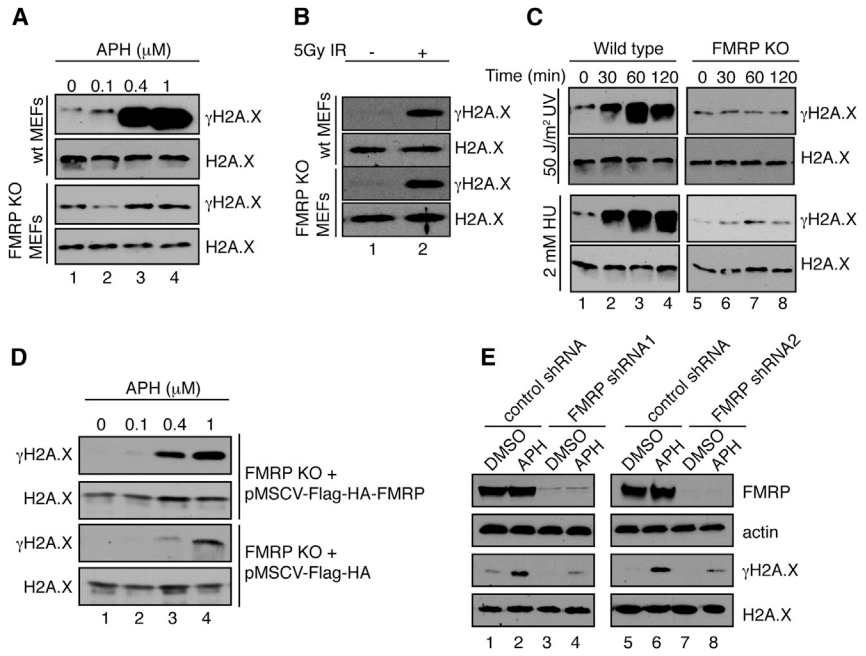

Figure 1. FMRP Modulates Histone H2A.X Phosphorylation Levels in Response to Replication Stress

(A) Wild-type (WT), but not FMRP KO, MEFs exhibited dose-dependent γH2A.X induction in response to APH (lanes 1–4). See also Figures S1A–S1C.

(B) WT MEFs and FMRP KO MEFs exhibited similar degrees of γH2A.X induction (5-fold) in response to 5 Gy of irradiation (lanes 1 and 2).

(C) WT, but not FMRP KO, MEFs exhibited time-dependent γH2A.X induction in response to 50 J/m^2 of UV irradiation or 2 mM of HU (10-fold induction at 60 min posttreatment; compare lanes 1–4 with lanes 5–8).

(D) FMRP KO MEFs reconstituted with WT Flag-HA-FMRP (pMSCV-Flag-HA-FMRP) or vector alone (pMSCV-Flag-HA) were exposed to various concentrations of APH. See also Figure S1D. pMSCV-Flag-HA-FMRP MEFs exhibited more pronounced γH2A.X induction compared with pMSCV-Flag-HA cells (12-fold in Flag-HA-FMRP cells and 4-fold in Flag-HA cells; lanes 1–4).

(E) FMRP RNAi HeLa cells, but not control cells, showed diminished γH2A.X induction in response to APH (3.4-fold and 8-fold, respectively; compare lanes 1/2 with 3/4, and 5/6 with 7/8). See also Figures S1E, S1F, and S2.

Nelson, 1994). Besides cognitive impairment, fragile X males also display macroorchidism (Johannisson et al., 1987; O'Donnell and Warren, 2002) and female *Fmr1* KO mice develop abnormal ovaries (Ascano et al., 2012), indicating an additional germline or gonadal effect of disruption of *Fmr1* expression.

Previous studies demonstrated a wide tissue distribution for FMRP and established it as largely a cytoplasmic protein, with only about 4% FMRP in the nucleus (Feng et al., 1997), where its function remains unknown. However, several reports suggested a potential role for FMRP in the nucleus. Studies in *Xenopus* and zebrafish showed that at 2–3 hr postfertilization, Fmrp is predominantly nuclear (Blonden et al., 2005; Kim et al., 2009; van 't Padje et al., 2005). In addition, Fmrp was found to decorate lampbrush chromosomes in *Xenopus* oocytes (Kim et al., 2009). Furthermore, nuclear FMRP interacting protein (NUFIP) associates with BRCA1 (Cabart et al., 2004), suggesting a potential functional relationship between FMRP and BRCA1 in the nucleus. FMRP has also been found in the PARP complexes, which heavily influence the DDR cascades (Helleday et al., 2005; Isabelle et al., 2010; Kedar et al., 2008). Interestingly, mice lacking the DNA topoisomerase TOP3β, which is part of FMRP-containing messenger ribonucleoprotein particles (mRNPs) and is implicated in neuronal development, display progressive reduction in fecundity and aneuploidy (Kwan et al., 2003; Stoll et al., 2013). The fact that FMRP is present in DDR complexes and is predominantly nuclear in some gametes and early embryos led us to speculate that FMRP might have a novel nuclear function in the DDR during development.

In this study, we provide evidence that FMRP has an important role in the nucleus, where it modulates the replication stress response at the chromatin interface. We show that FMRP regulates H2A.X phosphorylation, BRCA1 focus formation, and accumulation of single-strand DNA intermediates in a chromatin binding-dependent manner, and this nuclear role of FMRP is separable from its well-established role in translational regulation. We extend this nuclear function of FMRP to mammalian meiosis using mouse spermatocytes as a model. We show that FMRP decorates meiotic chromosomes and regulates γH2A.X induction, BRCA1 and ATR recruitment, and resolution of single-strand repair intermediates during meiosis. Taken together, our findings identify FMRP as a chromatin-binding protein and demonstrate that it plays a previously unanticipated role in the DDR at the chromatin interface, which is independent from the canonical role of FMRP in translational regulation.

RESULTS

Loss of FMRP Compromises Phosphorylation of H2A.X in Response to Replication Stress

In order to determine whether FMRP has a role in the DDR, we analyzed γH2A.X induction in cells that lack FMRP. We first treated wild-type and FMRP knockout (KO) mouse embryonic fibroblasts (MEFs) with increasing concentrations of the replication stress inducer aphidicolin (APH), which largely triggers single-strand breaks, and ionizing radiation, which generates DSBs (Brown and Baltimore, 2003; Rogakou et al., 1998; Zhou and Elledge, 2000). In wild-type but not FMRP KO, MEFs, APH-induced replication stress elicited an ~20-fold induction of γH2A.X (Figure 1A, compare lanes 1–4 of the first and third panels), indicating a requirement for FMRP in the replication stress response. In addition, FMRP KO MEFs showed reduced formation of γH2A.X foci upon treatment with APH as compared to wild-type MEFs (Figures S1A–S1C available online). In contrast, FMRP KO cells showed γH2A.X induction comparable

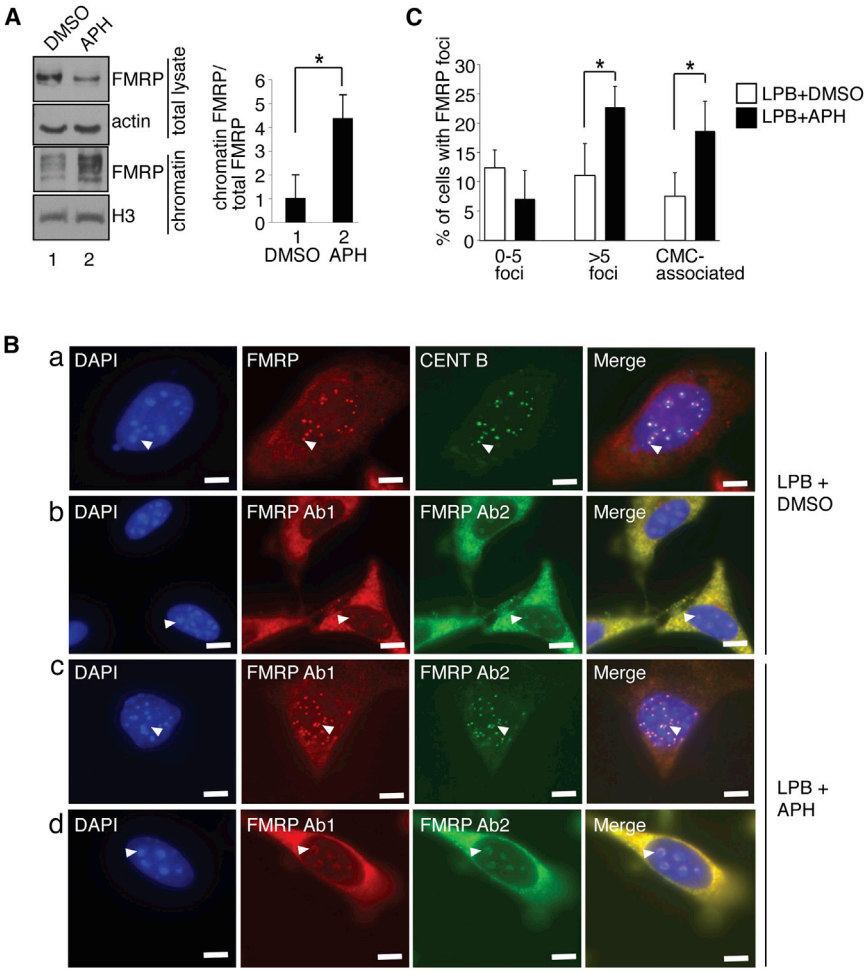

Figure 2. FMRP Chromatin Recruitment in Response to Replication Stress

(A) MEFs were treated with DMSO (lane 1) or APH (lane 2). Chromatin fractions were isolated and western blotted for FMRP. Bar graph, relative ratio of chromatin-associated FMRP to total FMRP. *$p < 0.05$, Student's t test. Data are an average of three independent experiments with SD.

(B) Immunostaining of nuclear FMRP in APH-treated or DMSO-treated MEFs in the presence of LPB. a: FMRP colocalized with CENT B next to CMCs. Arrowheads, representative colocalized FMRP (red) and CENT B (green) foci docked near CMCs. b: Representative FMRP signal (Ab-1: anti-FMRP [Abcam] antibody [red], Ab-2: anti-FMRP [Calbiotech] antibody [green]) enveloping CMCs in LPB-treated MEFs. c: Representative FMRP foci in LPB+APH-treated cells. d: representative FMRP signals enveloping CMCs in LPB+APH-treated MEFs. Arrowheads, selected FMRP foci wrapped around CMCs. Scale bar, 10 μm.

(C) APH treatment resulted in doubling of the number of cells with five or more FMRP foci (>5) or FMRP CMCs. *$p < 0.05$, Student's t test. Data are an average of three independent experiments with SD. See also Figure S3.

to that of the wild-type MEFs in response to ionizing radiation, indicating an intact response to DSB (Figure 1B, lane 2). In sum, FMRP KO MEFs showed distinct responses to different types of DNA damage, i.e., they responded to DSBs similarly to wild-type MEFs, but were defective in their response to replication stress.

To confirm that FMRP KO MEFs are defective in their response to replication stress, we subjected FMRP KO MEFs to additional sources of replication stress agents, including hydroxyurea (HU) and UV irradiation. In both cases, FMRP KO MEFs failed to show a time-dependent increase of the γH2A.X level as compared to wild-type MEFs (10-fold induction at 60 min posttreatment; Figure 1C, compare lanes 1–4 with lanes 5–8 of the upper and lower panels). Importantly, FMRP KO MEFs reconstituted with a FLAG-HA epitope-tagged, wild-type FMRP (Flag-HA-FMRP) conferred a more robust γH2A.X response to increasing concentrations of APH compared with the Flag-HA vector alone (Figures 1D and S1D; 12-fold induction in Flag-HA-FMRP cells as compared to 4-fold induction in Flag-HA only cells). This was not a MEF-cell-specific effect, since reduction of FMRP in HeLa cells by RNAi also resulted in a compromised induction of γH2AX in response to replication stress (Figure 1E). In addition to H2A.X phosphorylation regulation, loss of FMRP also affected another ATR-dependent, replication response-specific phosphorylation event: phosphorylation of BRCA1 at Ser-1423 (Tibbetts et al., 2000; Figures S1E and S1F). Consistent with the potential role of FMRP in the replication stress response, FMRP RNAi knockdown HeLa cells reconstituted with Flag-HA vector alone, but not tagged wild-type FMRP (Flag-HA-FMRP), were more sensitive to replication stress in the clonogenic survival assay (Figures S2A and S2B), and FMRP KO MEFs were also more sensitive to replication stress compared to wild-type MEFs (Figure S2C). These findings are in line with previous reports describing a prosurvival role of FMRP (Jeon et al., 2011, 2012; Liu et al., 2012). Taken together, the above findings link FMRP to replication stress-induced DDR and indicate that FMRP may be part of the ATR-dependent signaling pathway.

FMRP Is Recruited to Chromatin in Response to Replication Stress

Many proteins that function in the DDR are recruited to chromatin in response to DNA damage, where they participate in the DDR events (Bostelman et al., 2007; Conde et al., 2009; Krum et al., 2010; Pei et al., 2011; Wakeman et al., 2012; Wysocki et al., 2005). We therefore investigated the possibility that the FMRP may function in the replication stress response through recruitment to chromatin. By chromatin fractionation, we detected association of FMRP with chromatin, and this association was elevated by ~4-fold upon APH treatment (Figure 2A, compare lanes 1 and 2). Although biochemical fractionation allows detection of FMRP association with chromatin, direct

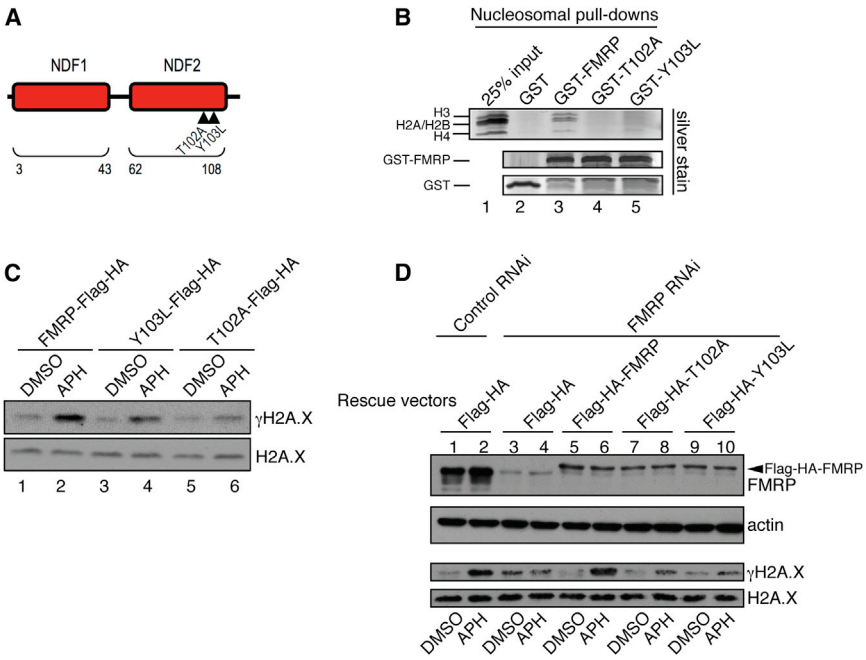

Figure 3. FMRP Docking to Chromatin Is Essential for FMRP-Dependent Modulation of γH2A.X Levels in Response to Replication Stress

(A) Diagram of Agenet$_{FMRP}$. Mutations T102A and Y103L are demarcated by triangles. See also Figure S4.

(B) GST-FMRP or GST-FMRP carrying mutations in Agenet$_{FMRP}$ (GST-T102A and GST-Y103L) were incubated with isolated nucleosomes. Pull-down material was run on gradient gels followed by silver staining. A complete set of core nucleosomal histones, including H3, H2A, H2B, and H4, were detected in WT, but not mutant, FMRP-mediated pull-downs (compare lanes 3–5). See also Figure S5A.

(C) WT FMRP (lanes 1 and 2) triggered more pronounced γH2A.X induction in FMRP KO MEFs in response to APH (12.8-fold) as compared with FMRP mutants (4-fold and 3-fold γH2A.X for Y103L and T102A mutants respectively; lanes 3–6). See also Figure S1D.

(D) FMRP RNAi in HeLa cells abolished γH2A.X induction in response to APH as compared with control RNAi (compare lanes 1/2 with lanes 3/4). Cotransfection with constructs expressing WT but not mutant forms of FMRP restored the induction of γH2A.X in FMRP RNAi cells in response to APH (compare lanes 5/6 with lanes 7/8 and 9/10). The slower-migrating band (in lanes 5–10) is Flag-HA-FMRP (indicated by an arrowhead).

visualization of FMRP in the nucleus is problematic due to the low level of nuclear FMRP (Figure S3A). However, it is possible to raise nuclear FMRP levels by using leptomycin B (LPB), which inhibits nuclear protein export (Tamanini et al., 1999). As shown in Figure 2B, in the presence of LPB, we detected FMRP foci in the vicinity of pericentromeric domains (chromocenters [CMCs]), which are easily recognizable in the mouse nuclei as large DAPI-positive domains (Figure 2B, a and b). Consistently, FMRP staining overlapped with the centromeric protein B (CENT B) signal, which marks pericentromeric heterochromatin (Figure 2B, a, arrowheads). In some cases, FMRP formed larger structures wrapped around the CMCs (Figure 2B, b, arrowheads). The number of cells with FMRP foci as well as CMC-associated FMRP domains increased 2-fold after APH treatment (Figures 2B, c and d, and 2C). In addition, we observed colocalization of FMRP and γH2A.X in MEFs treated with LPB (Figures S3B and S3C). Although the significance of FMRP colocalization with CENT B, CMCs, and γH2A.X foci requires further investigation, the above data nevertheless indicate that FMRP accumulates at specific chromatin domains and this accumulation can be increased upon replication stress, supporting our biochemical data (Figure 2A).

FMRP Binds Chromatin via Its N-Terminal Agenet Domain, and This Interaction Is Critical for FMRP Function in the DDR

What is the molecular basis for the observed chromatin association of FMRP? FMRP contains an N-terminal Agenet domain (Agenet$_{FMRP}$), which is a double-tudor domain that belongs to the Royal family of chromatin-binding proteins (Maurer-Stroh et al., 2003; Ramos et al., 2006). Interestingly, the Agenet domain was recently shown to bind histone substrates methylated at various lysine residues (Adams-Cioaba et al., 2010; Sabra et al., 2013). This led us to hypothesize that FMRP might target chromatin through its Agenet domain. Agenet$_{FMRP}$ consists of two adjacent Tudor domains, termed N-terminal domain of FMRP1 (NDF1) and N-terminal domain of FMRP2 (NDF2) (Ramos et al., 2006; Figure 3A). NMR studies identified residues T102 and Y103 on the surface of NDF2 as important for binding trimethylated lysine (Ramos et al., 2006; Figure 3A). Mutating T102 and Y103 to A and L, respectively (T102A and Y103L), significantly compromised FMRP binding to native nucleosomes isolated from HeLa cells (Figure 3B, compare lane 3 with lanes 4 and 5), indicating that Agenet$_{FMRP}$ is required for FMRP association with nucleosomal substrates. We next explored the possibility that methyl-lysine recognition is involved in FMRP binding to chromatin. We used a panel of recombinant *Xenopus* histones carrying methyl-lysine analogs at various positions (Simon et al., 2007) in in vitro binding reactions with Agenet$_{FMRP}$. Agenet$_{FMRP}$ did not show a significant interaction with unmethylated histone H3, but bound histone H3 containing methyl-lysine analogs at several positions (Figure S4A). Full-length FMRP also bound methylated, but not unmethylated, histone H3 (data not shown).

We next carried out microscale thermophoresis (MST) (Jerabek-Willemsen et al., 2011; Wienken et al., 2010) in order to understand the dynamics of Agenet$_{FMRP}$ binding to various histone methylation marks. Consistent with the biochemical binding data, we found that Agenet$_{FMRP}$ exhibited higher affinity for histone H3 carrying lysine methylation mimics, including H3Kc79me2 (K_d 135 ± 28 nM; Figure S4B) and H3Kc27me1 (K_d 102 ± 11 nM; Figure S4C) as compared with unmethylated H3 (K_d 1063 ± 136 nM; Figure S4D). Both the biochemical and

MST data suggest that $Agenet_{FMRP}$ preferentially binds methylated histone H3, but does not display significant methyl site specificity in vitro. Importantly, $Agenet_{FMRP}$ mutations that abolish FMRP binding to native chromatin (Figures 3A and 3B) also interfered with $AgenetKHKH_{FMRP}$ (Agenet and two adjacent nucleic acid binding domains) binding to the in vitro assembled methylated MLA nucleosomes (H3Kc79me2; Figure S5A, compare lanes 3–5). Collectively, these data demonstrate that $Agenet_{FMRP}$ is necessary and sufficient for FMRP binding to chromatin, which might involve a sequence-independent methyl-lysine recognition function of $Agenet_{FMRP}$.

FMRP Binding to Chromatin Is Required for FMRP-Dependent Modulation of γH2A.X Levels in Response to Replication Stress

We next carried out genetic complementation experiments to investigate potential functional roles of FMRP chromatin association in the DDR. FMRP KO MEFs were reconstituted with wild-type or mutant forms of FMRP (T102A and Y103L), which are compromised in their ability to bind nucleosomes. Wild-type FMRP (Figure 3C, lanes 1 and 2) was more effective than the mutant forms of FMRP (Figures 3C, lanes 3–6, and S1D, which shows comparable expression of wild-type and mutant FMRP proteins) in conferring the induction of H2A.X phosphorylation in the mouse FMRP KO MEF cells in response to APH treatment (12.8-fold γH2A.X increase with the wild-type FMRP and 4- and 3-fold γH2A.X increase with the Y103L and T102A mutants, respectively). Similar results were obtained with HeLa cells in which the endogenous FMRP was inhibited by RNAi, and which were then complemented with either the wild-type FMRP or the FMRP Agenet domain mutants. As shown in Figure 3D, wild-type FMRP conferred a significantly higher level of γH2A.X response (9-fold induction, compare lanes 5 and 6, third panel from the top) than the Agenet point mutants (T102A and Y103L; 3-fold γH2A.X induction, compare lanes 7 and 8, and lanes 9 and 10, third panel from the top). These findings suggest that the recruitment of FMRP to chromatin is critical for FMRP-dependent regulation of H2A.X phosphorylation.

FMRP Mutants Defective in Supporting H2A.X Phosphorylation Are Not Compromised in Their Ability to Modulate Translation-Dependent AMPAR Trafficking

FMRP has a well-documented role in regulating activity-dependent synaptic translation of a specific subset of mRNAs, which is important for the maintenance of synaptic plasticity (Bassell and Warren, 2008; Bear et al., 2004; Brown et al., 2001; O'Donnell and Warren, 2002). Previous studies showed that a reduction of FMRP in dendrites leads to an excessive internalization of the alpha-amino-3-hydroxy-5-methyl-4-isoxazole propionic acid receptor (AMPAR) subunit GluR1 (Nakamoto et al., 2007), which is a critical process for the maintenance of synaptic plasticity. This finding provided the foundation for the mGluR theory of fragile X syndrome (Bear et al., 2004). We asked whether the chromatin-binding-defective FMRP point mutants were also compromised in their ability to dampen AMPAR internalization. As expected, immunofluorescence staining showed that FMRP KO neurons exhibited less AMPAR signal remaining on the surface and more internalized AMPAR signal relative to wild-type neurons (Figure S5B, compare panels 1 and 2). Quantitatively, the ratio of internalized to total AMPARs was increased in neurons isolated from *Fmr1* KO mice as compared with wild-type neurons (Figure S5C, compare boxplots 1 and 2). Importantly, the FMRP chromatin-binding-defective mutants were able to rescue this AMPAR trafficking defect similarly to the wild-type FMRP (Figures S5B, panels 3–5, and S5C [compare boxplot 1 with boxplots 2 and 3–5]). These findings indicate that the newly identified role of FMRP in the DDR is mechanistically distinct from its canonical function in modulating synaptic strength.

FMRP Patient Mutant R138Q Is Defective in Mediating DDR Events, but Retains Normal Translation-Dependent AMPAR Internalization

Recently, a novel FMRP sequence variant, R138Q, was found in a developmentally delayed male without the typical CGG-repeat expansion in the 5′ UTR of the *FMR1* gene (Collins et al., 2010). Because the R138Q mutation lies near the extreme C terminus of $Agenet_{FMRP}$ (Figure S6A), we investigated whether this patient mutation affects FMRP nucleosomal binding. As shown in Figure 4A, the FMRP R138Q mutant failed to bind native nucleosomes (compare lanes 3 and 4) as well as recombinant H3Kc79me2 nucleosome (Figures 4B, S5A [lane 6], and S6B, which shows comparable levels of wild-type and R138Q recombinant proteins used for the binding assays). Importantly, the R138Q mutant also failed to confer γH2A.X induction in the FMRP KO MEFs in response to replication stress (Figures 4C [compare lanes 1–6 with lanes 7–12] and S6C, which shows comparable levels of expression of wild-type and R138Q reconstituted in the FMRP KO MEF cells). In addition to the γH2A.X defect, the R138Q FMRP mutant did not effectively support the formation of BRCA1 foci and phosphorylation of BRCA1 at Ser-1423 in FMRP KO MEFs in response to APH treatment as compared with wild-type FMRP (Figures 4D–4G and S6D). In addition, we observed an increased incidence of single-strand DNA intermediates (as indicated by RPA32 staining) in FMRP KO MEFs rescued with the R138Q mutant as compared with wild-type FMRP, suggesting a repair defect (compare Figures 4H and 4I; quantification in Figures 4J and 4K). Importantly, RPA32 staining associated with CMCs was also increased in FMRP KO MEFs complemented with R138Q, suggesting a possible functional significance of FMRP targeting to CMCs in the context of the DDR (Figures 4H and 4I, bottom, arrows). FMRP KO MEFs reconstituted with the R138Q mutant were also more sensitive to increasing concentrations of HU as compared with wild-type FMRP reconstituted cells in the clonogenic survival assay (Figure S6E). In contrast, the FMRP R138Q mutant functioned similarly to wild-type FMRP in suppressing excessive AMPAR internalization in FMRP KO neurons (Figure S6F [compare panels 3 and 4] and S6G [compare boxplots 3 and 4]). Taken together, these results suggest the tantalizing possibility that abrogation of this newly identified nuclear function of FMRP in the DDR may lead to a DDR-dependent clinical phenotype.

FMRP Is Loaded onto Chromosomes during Male Meiosis and Regulates Placement of γH2AX

The above findings provide strong support for a role of FMRP in the DDR via its association with chromatin. However, the

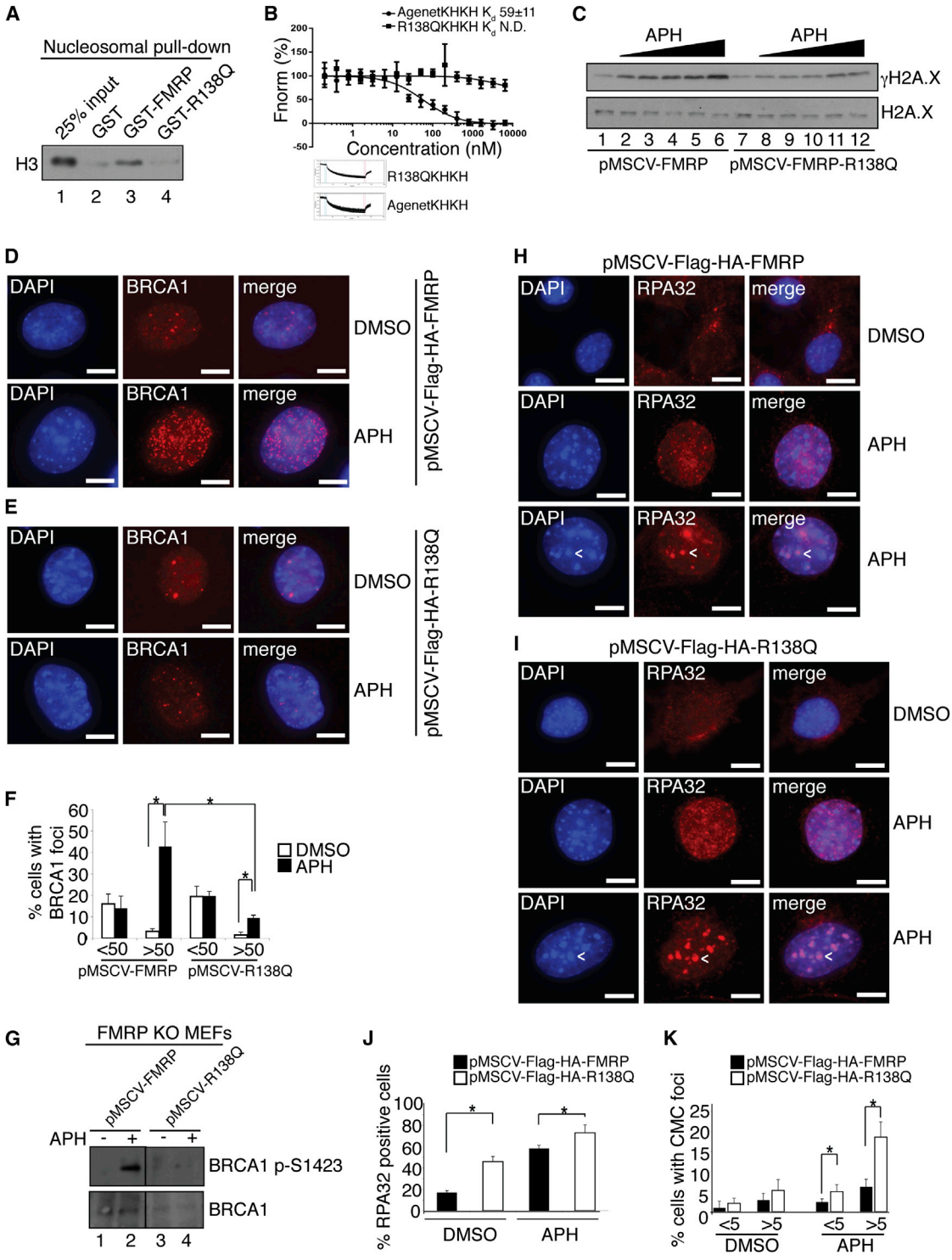

Figure 4. Patient Mutant R138Q Is Defective in γH2A.X Induction and BRCA1 Foci Formation and Promotes Excessive RPA Retention on Chromatin

(A) Unlike WT FMRP, the R138Q FMRP mutant failed to bind nucleosomes in vitro (compare lanes 3 and 4).

(B) Equilibrium binding analysis using recombinant MLA nucleosomes dimethylated at H3K79 and WT AgenetKHKH (K_d = 59 nM) or R138QKHKH (binding not detected). See also Figures S5A and S6B.

(C) FMRP KO MEFs rescued with WT FMRP, but not the R138Q FMRP patient mutant, exhibited a dose-dependent γH2A.X response triggered by APH (0.05 μM, 0.1 μM, 0.3 μM, 0.5 μM, 1 μM). See also Figure S6C.

(legend continued on next page)

biological significance of this finding was unclear. In this regard, mammalian meiosis represents perhaps the most relevant biological process in which extensive DNA damage and recombinogenic events normally occur. In wild-type meiotic cells, DSBs are generated during prophase by the topoisomerase-like enzyme SPO11, and form sites for homologous recombination and crossing over. DSBs accumulate γH2A.X and recruit many components of the somatic DDR machinery, including ATR and BRCA1. Repair then occurs in a highly regulated fashion, accompanied by pairing of homologous chromosomes (synapsis) and recombination between homologs (Blanco-Rodríguez, 2012; Garcia-Cruz et al., 2009; Turner et al., 2004, 2005). Importantly, in addition to defects in synaptic signaling in neurons, male fragile X patients exhibit macroorchidism and *Fmr1* KO mouse ovaries display premature follicular overdevelopment (Ascano et al., 2012; Turner et al., 1975, 1980). Meiotic germ cells are therefore a relevant biological context in which to analyze the association of FMRP with chromatin in the DDR in vivo.

We used a mouse *Fmr1* KO model to investigate whether FMRP is associated with chromatin and the DDR during mammalian meiosis. All mouse experiments were approved by the animal care and use committee at the appropriate institution. We first asked whether FMRP is present in the germ cell nucleus during meiosis. We performed immunostaining on chromosome spreads of adult male spermatocytes in meiotic prophase. Strikingly, we identified distinct FMRP puncta on condensed pachytene-stage chromosomes (Figure 5A). These puncta were aligned along the chromosomes, as visualized by costaining for the synaptonemal complex (SC) component SYCP1. FMRP puncta were not found on the chromosomes in *Fmr1* KO cells, confirming the specificity of the antibody staining (Figure S7A). We conclude that FMRP is present in the nucleus during meiotic pachytene and is localized on or near the chromatin at this stage.

In wild-type meiotic cells, γH2A.X accumulates throughout the nucleus during the leptotene and zygotene stages of prophase concomitantly with DSB formation, but is removed from the chromosomes as repair proceeds and is absent from the autosomes by the pachytene stage. In males, the X and Y chromosomes retain γH2A.X during pachytene because these two chromosomes lack homologs and cannot fully synapse, and repair is delayed (Handel and Schimenti, 2010). Analogously, in mutants with defective repair and synapsis machinery, γH2A.X and other components of the DDR pathway are retained at unrepaired regions on the autosomes (Turner et al., 2005). We asked whether deposition of γH2A.X during meiotic prophase was impaired in *Fmr1* KO cells. *Fmr1* KO spermatocytes exhibited two distinct defects in γH2A.X accumulation: (1) reduced deposition of γH2A.X during the leptotene stage, and (2) inappropriate retention of γH2A.X on autosomes during pachytene (Figure 5B). This phenotype was not the result of delayed or impaired formation of DSBs, since there was no difference in SPO11 staining between wild-type and KO cells (Figure S7B). These defects were evident in only a subset of cells (Figure 5C), perhaps explaining the preserved fertility of the *Fmr1* KO males.

Fmr1 Mutant Mice Exhibit Defective Chromosome Synapsis and Defective Resolution of Single-Strand Intermediates during Meiotic Prophase

In wild-type meiotic cells, the RAD51 homolog DMC1 associates with the single-strand intermediates produced during DSB repair and facilitates invasion of the homologous chromosome, allowing recombination (Pittman et al., 1998; Schwacha and Kleckner, 1997; Yoshida et al., 1998). This process occurs during the zygotene stage and is largely complete by pachytene, by which time most DMC1 has dissociated from the chromosomes. Successful strand invasion catalyzed by DMC1 is required to proceed with repair and crossing over, including recruitment of the MLH1/MLH3 heterodimer during middle to late pachytene (Moens et al., 2002; Pittman et al., 1998; Yoshida et al., 1998). To determine whether single-strand intermediates were resolved in meiotic cells in the absence of FMRP, we costained pachytene nuclei with DMC1 and MLH1. We found that *Fmr1* KO midpachytene spermatocytes inappropriately retained high levels of DMC1 on the chromosomes (Figures 6A and 6B), associated with reduced recruitment of MLH1 (Figures 6A, 6C, and 6D). These findings suggest that resolution of single-strand DNA repair intermediates is delayed in meiotic germ cells in the absence of FMRP, resulting in impaired crossover formation.

Consistent with a failure to repair DNA breaks, we found that BRCA1 and ATR were also inappropriately retained on the chromosomes in pachytene spermatocytes. BRCA1 and ATR were restricted to the unpaired X and Y chromosomes in wild-type spermatocytes, but were present on regions of the autosomes in *Fmr1* KO spermatocytes (Figures 7A–7C). BRCA1 and ATR staining on the sex chromosomes was also

(D and E) BRCA1 foci formation in FMRP KO MEFs rescued with WT FMRP (D) in response to APH was more pronounced as compared with FMRP KO MEFs rescued with the R138Q FMRP patient mutant (E). See also Figure S6D.
(F) Forty percent of FMRP KO MEFs rescued with WT FMRP exhibited >50 BRCA1 foci per cell upon APH treatment, compared with 10% in MEFs rescued with the R138Q patient mutant.
(G) BRCA1 S1423 phosphorylation in FMRP KO MEFs rescued with WT FMRP in response to APH was more pronounced as compared with rescue with the R138Q FMRP patient mutant (compare lanes 2 and 4).
(H and I) RPA32 foci formation in FMRP KO MEFs rescued with WT FMRP in response to APH was less pronounced as compared with FMRP KO MEFs rescued with the R138Q patient mutant (compare middle panels in (H) and (I). Note the accumulation of a subset of RPA32 foci at CMCs (arrowheads, lower panels).
(J and K) Quantification of total (J) and CMC-associated (K) RPA32 foci in FMRP KO MEFs rescued with WT FMRP and R138Q patient mutant in response to APH. The percentage of cells positive for RPA32 increased from 10% to 50% upon APH treatment after rescue with WT FMRP, and from 40% to 70% after rescue with the R138Q mutant. Note increased numbers of RPA32-positive cells in the case of R138Q mutant rescue MEFs even in the absence of APH treatment.
(K) Seventeen percent of R138Q mutant rescue MEFs and 6% of WT FMRP rescue MEFs had more than five CMC-associated RPA32 foci upon APH treatment.
*$p < 0.05$, Student's t test. Data are an average of three independent experiments with SD. Scale bars, 10 μm.
See also Figure S6D.

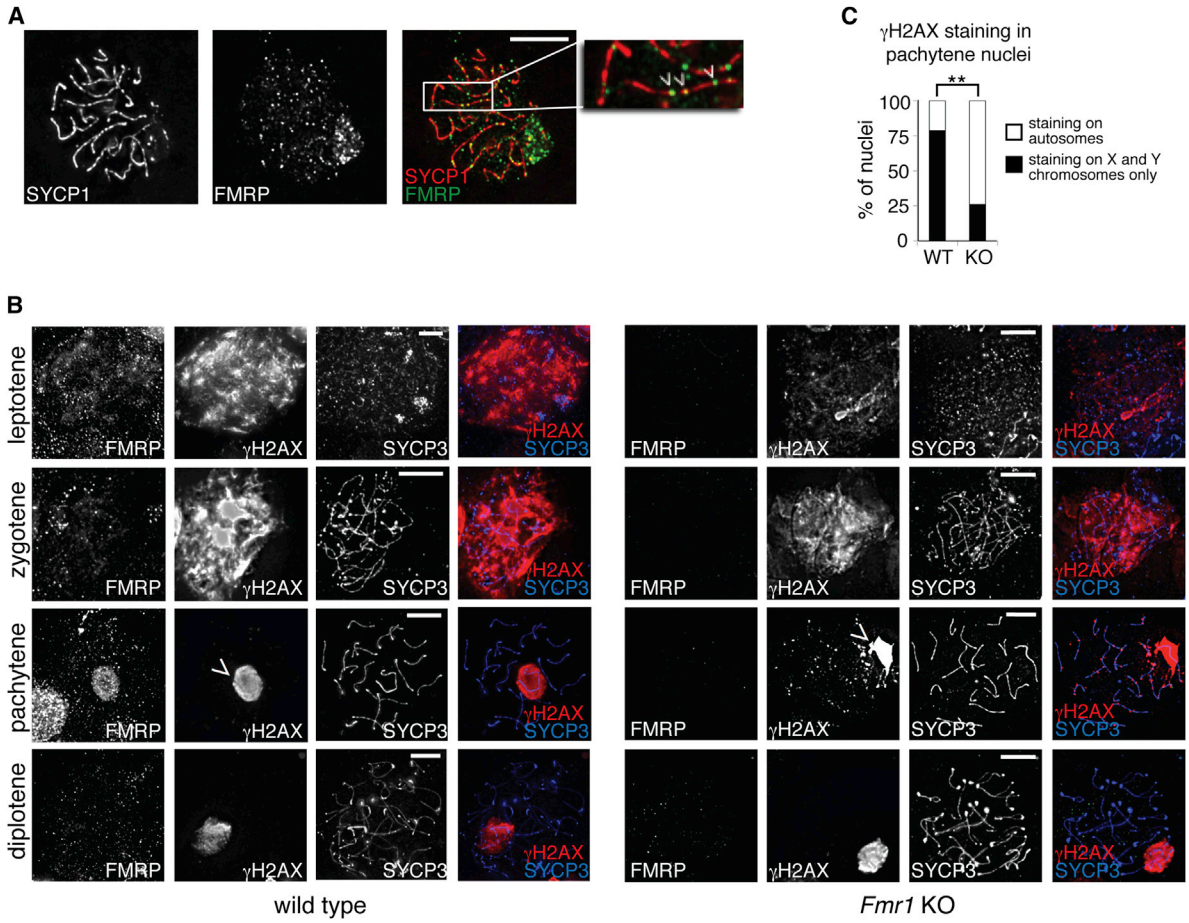

Figure 5. FMRP Is Present on Meiotic Chromosomes and Regulates Placement of γH2A.X

Immunofluorescence staining was performed on spread chromosomes from adult male primary spermatocytes, and cells were imaged by deconvolution microscopy.

(A) Pachytene stage nucleus showing FMRP puncta along the chromosomes. SYCP1 marks the full length of the autosomes during the pachytene stage. Inset shows FMRP puncta (green) aligned along SYCP1-stained chromosomes (red). See also Figure S7A.

(B) γH2A.X and FMRP staining in WT (left) and *Fmr1* KO (right) primary spermatocyte nuclei at leptotene, zygotene, pachytene, and diplotene stages of meiotic prophase. SYCP3 accumulates on chromosomes beginning in leptotene and is present along their full length during pachytene. In *Fmr1* KO cells, accumulation of γH2A.X is delayed in the leptotene stage. At the pachytene stage, γH2A.X is restricted to the sex chromosomes (arrowheads) in WT cells, but remains at some autosomal locations in *Fmr1* KO cells. Scale bars, 10 μm.

(C) Percentage of cells retaining γH2A.X outside of the sex chromosomes in WT and KO pachytene spermatocytes. **$p < 0.01$, Fisher's exact test. See also Figure S7B.

discontinuous in *Fmr1* KO spermatocytes, but continuous in wild-type cells. Similar to the defects in γH2A.X deposition, DMC1 retention, and MLH1 recruitment, these BRCA1 and ATR localization phenotypes varied between cells: some KO cells exhibited autosomal BRCA1 and ATR staining, whereas others resembled wild-type cells (Figure 7C).

Because failure to resolve DSBs and to form interhomolog crossovers is also associated with defective synapsis, we next asked whether *Fmr1* KO spermatocytes also displayed synapsis defects. SYCP3, a lateral element of the SC, assembles on unpaired chromosomes during early prophase, whereas SYCP1, a central element of the SC, assembles only on synapsed chromosomes (Fraune et al., 2012). We found that whereas wild-type pachytene nuclei had continuous SYCP1 staining along the chromosomes, many *Fmr1* KO nuclei had discontinuous SYCP1 staining, indicating that SC formation was not complete (Figure 7D; Bishop et al., 1992; Pittman et al., 1998; Yoshida et al., 1998). Taken together, these findings suggest that resolution of single-strand repair intermediates, crossing over, and subsequent pairing of homologous chromosomes during meiotic prophase are incomplete in a subset of spermatocytes lacking FMRP.

Histone H3K79 Methylation Plays a Role in the Recruitment of FMRP to Chromatin In Vivo

As described above, both the $Agenet_{FMRP}$ and a full-length FMRP bind histone substrates in a methyl-lysine-dependent manner (Figure S4 and data not shown). However, it remains

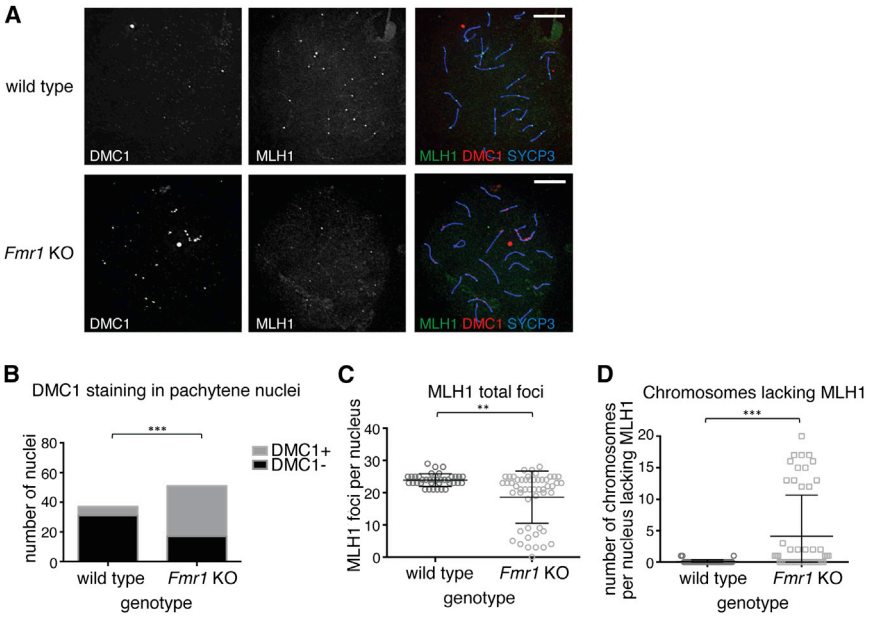

Figure 6. *Fmr1* KO Spermatocytes Exhibit DNA Repair Defects and Delayed Resolution of Single-Strand Intermediates at the Pachytene Stage

Staining of chromosome spreads was performed as in Figure 5.

(A) Costaining of DMC1, MLH1, and the SC component SYCP3, showing retention of DMC1 and reduction of MLH1 in *Fmr1* KO cells at midpachytene.

(B) Numbers of WT and KO cells positive for DMC1 staining at midpachytene. ***$p < 0.0001$, Fisher's exact test.

(C) MLH1 foci per midpachytene nucleus in WT and KO. **$p < 0.01$, Mann-Whitney U test.

(D) Number of chromosomes per midpachytene nucleus lacking MLH1 foci. In WT cells, there is at least one MLH1 focus per chromosome. ***$p < 0.0001$, Mann-Whitney U test. Scale bars, 10 μm.

unclear whether FMRP binds methyl histones with some specificity in vivo and which methyltransferases are necessary for FMRP chromatin recruitment. Dot1, the H3K79 methyltransferase, has been shown to play a role in yeast meiosis (Ontoso et al., 2013; San-Segundo and Roeder, 2000). In addition, recent reports demonstrated an increase in H3K79me2 and H3K79me3 levels in mouse spermatocytes in pachytene, with H3K79me3 specifically enriched at the sex chromosomes and centromeres (Ontoso et al., 2014). As a first step toward understanding the role of histone methylation in FMRP recruitment, we generated mice conditionally lacking DOT1L (*Dot1L* cKO; Figures S7C–S7E; Bernt et al., 2011), the only known mammalian H3K79 methyltransferase, in the germ cells, and stained meiotic spreads for FMRP. We found a small but significant reduction in the number of chromatin-associated FMRP puncta in the *Dot1L* cKO. This effect was especially evident on the X and Y chromosomes, where FMRP is particularly abundant during pachytene (Figures 7E and 7F). Importantly, similar to FMRP KO MEFs, *Dot1L* mutant MEFs exhibited reduced γH2A.X foci formation in response to APH (Figure S1C, right) as well as an increased sensitivity to increasing concentrations of APH compared with wild-type MEFs (Figure S2C). We conclude that methylated H3K79 might function in the same DDR pathway as FMRP and help to recruit or retain FMRP at chromatin associated with DNA damage repair intermediates.

DISCUSSION

We have identified FMRP as a chromatin-binding protein and uncovered a novel and unanticipated function for FMRP in the nucleus, where it regulates the DDR. In addition, we uncovered a biological role for the DDR function of FMRP during mammalian spermatogenesis. We provide strong evidence that the Agenet domain binds histone H3 in a methylation-dependent manner, without displaying an overt preference toward a specific methyl-lysine site. Conceivably, however, the binding specificity could be enhanced in vivo. Our preliminary data consistently showed that the histone H3K79 methyltransferase DOT1L is important for FMRP chromatin association during meiosis, suggesting that H3K79 methylation may play a role in FMRP chromatin targeting in vivo. Our current data do not exclude the possibility that FMRP may also be capable of binding other methylated targets, such as nucleic acids.

This newly identified function of FMRP in the replication stress response appears to be independent of the classical role of FMRP in maintaining synaptic plasticity via translational regulation. Instead, nuclear FMRP may function in the DNA repair pathways through chromatin association. Our finding is consistent with published observations, including the report that FMRP interacts with poly(ADP-ribose) glycohydrolase (PARG) and poly (ADP-ribose) polymerase (PARP), which are major modulators of genomic stability (Gagné et al., 2005; Isabelle et al., 2010, Ciccia and Elledge, 2010; Haince et al., 2007). The fact that the DNA topoisomerase TOP3β is present in FMRP-containing mRNPs, is involved in neuronal development and genomic stability, and contributes to germ cell development suggests yet another intriguing connection between FMRP and the DDR. It is interesting to note that similar to FMRP, TOP3β is also associated with XY bivalents during pachytene (Kwan et al., 2003). We speculate that FMRP performs a docking function to regulate the chromatin accessibility of DDR proteins. Although the detailed molecular mechanisms of FMRP-dependent DDR await further clarification, our data on the connection of FMRP with chromatin in the DDR represent an important advance in our understanding of FMRP function.

Importantly, DDR events such as γH2A.X induction and ATR/BRCA1 signaling heavily influence meiosis, specifically crossover formation and synapsis (Turner et al., 2004, 2005). Defects in synapsis can lead to chromosome nondisjunction, resulting in impaired gamete development or the generation of aneuploid gametes and developmental defects in the resulting embryo (Handel and Schimenti, 2010). Our findings suggest that the

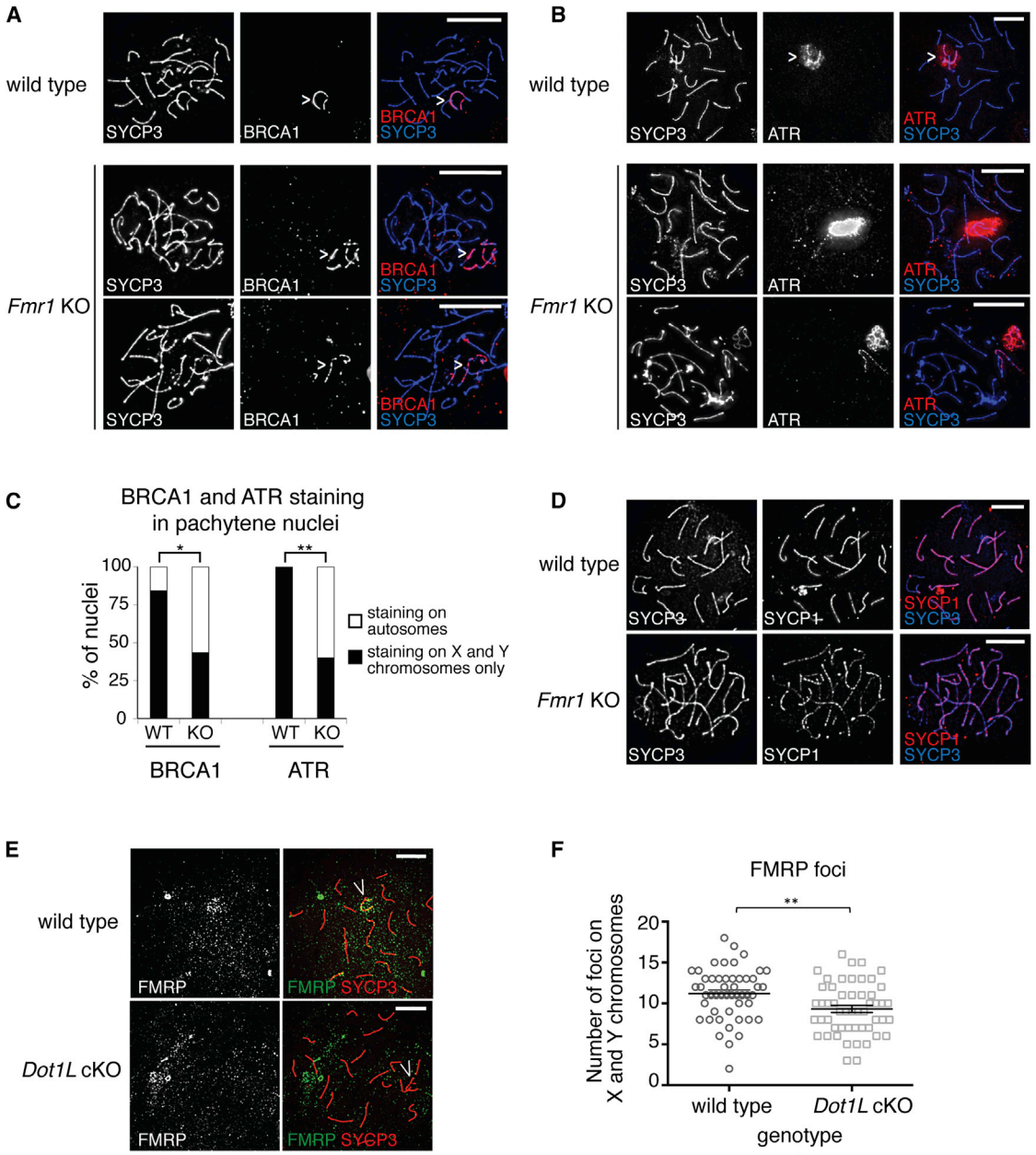

Figure 7. Abnormal BRCA1 and ATR Loading and Synapsis Defects in *Fmr1* KO Spermatocytes

(A) Sample images of BRCA1 staining in pachytene spermatocytes in WT and KO animals. In WT, BRCA1 staining is continuous and restricted to the sex chromosomes (arrowhead). In KO, it is discontinuous and frequently present on the autosomes. SYCP3 marks the chromosomes.

(B) Sample images of ATR staining in pachytene spermatocytes in WT and KO animals. In WT, ATR staining forms a cloud around the sex chromosomes (arrowhead) and is absent from the autosomes. In KO, ATR staining is retained in puncta on the autosomes and sometimes coats a complete autosome (bottom panels). SYCP3 marks the chromosomes.

(C) Percentage of cells that retained BRCA1 or ATR outside of the sex chromosomes in WT and KO spermatocytes. *$p < 0.05$; **$p < 0.01$, Fisher's exact test.

(D) Costaining of lateral (SYCP3) and central (SYCP1) elements of the SC shows discontinuous SYCP1 staining in *Fmr1* KO cells, indicating defective SC formation.

(E and F) Methylated H3K79 helps to recruit FMRP to chromatin.

(E) Staining of FMRP in pachytene spermatocyte spreads from WT and *Dot1L* cKO mutants. Chromosome-associated FMRP signal is reduced in cKO cells, especially near the X and Y chromosomes. SYCP3 marks the chromosomes.

(F) Quantitation of X- and Y-chromosome-associated FMRP foci. **$p < 0.01$, unpaired t test. Scale bars, 10 μm.

See also Figures S1C and S7C–S7E.

rate of germline chromosomal instability among *Fmr1* KO mice or fragile X patients at sites outside the fragile X locus may be elevated. This hypothesis is supported by a recent study that described increased rates of DNA damage and apoptosis in spermatocytes of *Fmr1* KO mice (Tian et al., 2013). In addition, low FMRP levels were correlated with spermatogenesis defects in patients with maturation arrest (Tian et al., 2013). Thus, our findings provide a potential molecular mechanism for the DNA damage, apoptosis, and spermatogenesis defects observed in mice and patients lacking FMRP.

Interestingly, in yeast *Dot1* mutants, meiotic cells exhibit increased levels of unrepaired DNA damage and proceed through sporulation to produce mature spores with poor viability (San-Segundo and Roeder, 2000). In mouse spermatocytes, DOT1L chromatin loading and H3K79 methylation are dynamically regulated during meiosis. In particular, H3K79me3 and DOT1L protein accumulate at the sex chromosomes, and H3K79me3 accumulates at centromeres during the pachytene stage (Ontoso et al., 2014). Our finding that FMRP is depleted at the sex chromosomes in *Dot1L* conditional mutants supports an interaction between FMRP and methylated histones during meiosis, and raises the possibility that H3K79 methylation may be important for FMRP chromatin association in vivo. Interestingly, the Tudor domain of Survival Motor Neuron protein (SMN), which carries a methyl-lysine interacting surface similar to that of the FMRP Agenet domain (Ramos et al., 2006), was recently shown to interact with H3K79me1/2 in a DOT1L-dependent manner (Sabra et al., 2013)

Macroorchidism is a hallmark of fragile X syndrome, but little is known with respect to its etiology. Malformed spermatids have been observed in both human fragile X patients and *Fmr1* KO mice, suggesting a defect in sperm development (Slegtenhorst-Eegdeman et al., 1998; Johannisson et al., 1987). Adult male patients carrying the full fragile X repeat expansion produce sperm that carry a contracted premutation but never the full expansion (Reyniers et al., 1993), implying that sperms carrying a full mutation are selected against at a premeiotic stage, allowing only those with a contracted *FMR1* repeat to reach maturity (Bächner et al., 1993; Malter et al., 1997). Our finding that spermatocytes lacking FMRP exhibit defects in chromosome synapsis during meiotic prophase lends support to this model, and suggests a mechanism for this effect.

The idea of a functional involvement of FMRP in the DDR is especially appealing given recent evidence pointing to FMRP as a prosurvival protein. The absence of FMRP promotes apoptosis (Jeon et al., 2011) and telomere erosion in fragile X patients, which is a major hallmark of genomic instability (Jenkins et al., 2008). In addition, fragile X patients have been reported to display a lower incidence of cancer (Schultz-Pedersen et al., 2001), whereas an increase in FMRP levels promotes tumor metastasis (Lucá et al., 2013). Lastly, given that the loss of FMRP function leads to a common form of intellectual disability and autism, it is tempting to speculate that the role of FMRP in the DDR might represent a novel, previously unappreciated contributing factor in the development of fragile X syndrome. Interestingly, a forward genetic screen in *Drosophila* identified 26 missense mutations in the N terminus of dFMRP that affect axonal development (Reeve et al., 2005). Some of these mutations are localized to the dFMRP Agenet domain and are predicted to impact the ability of dFMRP to bind chromatin. It has been suggested that the Agenet domain may also play a role in the translation-independent function of FMRP in synaptic signaling (Deng et al., 2013). Therefore, it remains to be determined whether, in addition to its role in germ cell meiosis reported here, this nuclear function of FMRP also affects neuronal development, and whether the loss of FMRP has any DDR-related consequences in patients with fragile X syndrome.

EXPERIMENTAL PROCEDURES

Native Nucleosome Binding Reactions

Reactions were performed in the presence of binding buffer (50 mM Tris pH 7.5, 150 mM NaCl, 2 mM $MgCl_2$, 0.1% Triton X-100) using 100 ng of glutathione S-transferase (GST) fusion proteins and 5 μg of native nucleosomes isolated from HeLa cells at +4°C, and rotated for 2 hr before addition of glutathione agarose beads (GE Healthcare). Beads were washed four times with binding buffer. Three independent experiments were performed.

MLA Nucleosome Binding Reactions

Mononucleosomes were prepared as described previously (Lu et al., 2008). The reactions were performed similarly to native nucleosome binding reactions, but using 2 μg of MLA nucleosomes. Three independent experiments were performed.

γH2A.X Induction Rescue Experiments

HeLa cells were transfected with FMRP small hairpin RNA (shRNA) or control scramble shRNA. Scramble shRNA was cotransfected with empty backbone vector (POZ-Flag-HA). FMRP shRNA was cotransfected with Flag-HA vector alone or with rescue vectors expressing either wild-type or mutant forms of FMRP (Flag-HA-FMRP, Flag-HA-T102Y, or Flag-HA-Y103L). At 3 days post-transfection, cells were treated with DMSO or APH (0.5 μM) for 24 hr and then lysed in SDS sample buffer. Samples were subjected to western blotting. FMRP KO MEF rescue experiments were performed identically to HeLa rescue experiments, except that rescue constructs were introduced into cells using the pMSCV-Flag-HA viral system. Three independent experiments were performed.

FMRP Chromatin Recruitment Experiments

Chromatin fractionation experiments were adopted from Méndez and Stillman (2000). Briefly, after 1 μM APH treatment of MEFs for 24 hr, chromatin was isolated by resuspending cells in buffer A (10 mM HEPES [pH 7.9], 10 mM KCl, 1.5 mM $MgCl_2$, 1 mM dithiothreitol [DTT], 3 mM EDTA, 0.5% Triton X-100, and protease inhibitor cocktail [Roche]) and nuclei were collected by low-speed centrifugation (4 min, 1,300 × *g*), washed once in buffer A, and lysed in buffer B (3 mM EDTA, 0.2 mM EGTA, 1 mM DTT, and protease inhibitor cocktail [Roche]). Insoluble chromatin was collected by centrifugation (4 min, 1,700 × *g*), washed again in buffer B, and centrifuged again. The final chromatin pellet was resuspended in Laemmli buffer, sonicated, and boiled for 15 min. Total protein lysate for determination of total protein levels was aliquoted from cells still resuspended in buffer A. All procedures were performed at +4°C. Three independent experiments were performed.

Immunofluorescence Experiments

MEFs were treated with 10 ng/ml of LPB for 24 hr in the presence or absence of 0.5 μM APH. Cells were then fixed with ice-cold methanol, stained with the antibodies of interest, and mounted using DAPI mounting medium (Vectashield). MEFs were counted according to the number of nuclear FMRP foci or large CMC-associated FMRP domains (CMCs) after LPB+DMSO or LPB+APH treatment (24 hr). When Bethyl anti-BRCA1 and anti-RPA32 rabbit antibodies were used for staining, cells were extracted with CSK buffer (10 mM HEPES pH 7.4, 300 mM sucrose, 100 mM NaCl, 3 mM $MgCl_2$, 0.5% Triton X-100) for 30 min at room temperature and then fixed in 4%

paraformaldehyde (PFA) for 10 min, followed by washes in PBS and immunostaining. A total of 100 cells were counted in three independent experiments.

Preparation of Meiotic Chromosome Spreads

Male *Fmr1*^{KO}/Y and +/Y or *Dot1L* $^{\Delta/\Delta}$ and *Dot1L*$^{fl/+}$ littermates were sacrificed at 7 weeks of age. At least two individuals of each genotype were used for each experiment. The spread preparation protocol was modified from Peters et al. (1997). Testes were immersed in Dulbecco's modified Eagle's medium and the tunicae were removed. The separated tubule suspension was spun for 8 min at 1,000 × *g*, and cells were resuspended in 1 ml hypo-buffer (30 mM Tris-HCl pH 8.2, 50 mM sucrose pH 8.2, 17 mM sodium citrate) and incubated for 7 min at room temperature. The cell suspension was split into five tubes and spun for 8 min at 1,000 rpm. It was then resuspended in 170 μl 0.1 M sucrose and dropped onto the slides, and allowed to spread for 2–3 hr. Slides were prepared with 1% PFA with 0.1% Triton X-100, pH 9.2. For staining, slides were blocked in 3% BSA for 1 hr, incubated with primary antibody in 1% BSA overnight at 4°C, and then incubated with secondary antibody in 1% BSA for 1 hr at room temperature. Imaging was performed on a DeltaVision Elite deconvolution imaging system (Applied Precision) at 60× or 100× magnification. Stacks were compressed and analyzed using ImageJ software. The morphology of SYCP3-stained chromosomes was used to determine the stage of prophase.

For further details regarding the materials and methods used in this work, see Extended Experimental Procedures.

SUPPLEMENTAL INFORMATION

Supplemental Information includes Extended Experimental Procedures and seven figures and can be found with this article online at http://dx.doi.org/10.1016/j.cell.2014.03.040.

AUTHOR CONTRIBUTIONS

R.A. and Y.S. designed the study and cowrote the manuscript. R.A. analyzed the data, performed histone pull-downs, cloning, mutagenesis, in vitro binding experiments, microscale thermophoresis, FMRP RNAi experiments, DNA damage experiments, MEF reconstitution experiments, survival assays, chromatin recruitment experiments, and immunofluorescence experiments. B.J.L. performed experiments using *Fmr1* KO and *Dot1L* cKO mice, performed meiotic chromosome spreads and immunostaining, analyzed data, and cowrote the manuscript. M.N.K. performed AMPAR internalization experiments and data analysis, and contributed to the writing of the manuscript. A.B. performed BRCA1 rescue experiments. S.C., M.A., and C.X. performed in vitro binding assays with MLA histones, histone peptides, FMRP, and Agenet. J. Murn developed FMRP KO rescue cell lines. S.P. analyzed MST data. M.D.S., K.J.A, and A.S. designed and assembled MLA nucleosomes. C.R.V. developed *Dot1L* mutant MEFs and commented on the manuscript. T.G.K. and J. Min supervised histone peptide binding assays. W.F. and R.E.K. supervised nucleosome binding and commented on the manuscript. D.C.P. and S.T.W. supervised experiments and contributed to the writing of the manuscript. Y.S. supervised and directed the studies.

ACKNOWLEDGMENTS

We thank S. Elledge and B. Yankner for advice and helpful suggestions; A. Ciccia for help with DNA damage experiments; D. Reinberg and P. Voigt for help with nucleosomal preparations; J. Griesbach, A. Lazic, and S. Duhr from NanoTemper Technologies, and K. Yamagata, Y. Zheng, and X. Shang for help with microscale thermophoresis and kinetic data analysis; and E. Greer, A. Alekseyenko, and G. Shanower for logistical support. We also thank J. Mowrey, S. Ceman, S. Keeney, and U. Fischer for reagents; M. Bear for *Fmr1* KO mice; S. Armstrong for *Dot1L*$^{fl/fl}$ mice; K. Luger, G. Narlikar, S. Ceman, and U. Fischer for helpful comments; and M. Goodheart, D. Cooper, E. Derby, L. Elow, K. Igarashi, L. Kolinski, L. Pomponi, and M. Schuck for technical assistance. We also thank our collaborators who contributed to this project but whose work was not included in the manuscript: B. Ren, U. Wagner, and the Ren laboratory for FMRP genome-wide analysis; K. Zhao and his group for H3K79me2 genome-wide analysis; A. Vaquero for Suv39h double-null MEFs; and G. Schotta and T. Jenuwein for Suv4-20h double null MEFs. This work was supported by NIH grants NCI118487 and MH096066 to Y.S., National Research Training Grant AG00222-7 to R.A., NRSA grant HD075591 and a Hope Funds for Cancer Research postdoctoral fellowship to B.J.L., and HHMI funding to D.C.P., and in part by NIH grants HD020521 and HD024064 to S.T.W. Y.S. is an American Cancer Society Research Professor, and is a cofounder of Constellation Pharmaceuticals and a member of its scientific advisory board.

Received: May 31, 2013
Revised: February 4, 2014
Accepted: March 20, 2014
Published: May 8, 2014

REFERENCES

Adams-Cioaba, M.A., Guo, Y., Bian, C., Amaya, M.F., Lam, R., Wasney, G.A., Vedadi, M., Xu, C., and Min, J. (2010). Structural studies of the tandem Tudor domains of fragile X mental retardation related proteins FXR1 and FXR2. PLoS ONE *5*, e13559.

Ascano, M., Jr., Mukherjee, N., Bandaru, P., Miller, J.B., Nusbaum, J.D., Corcoran, D.L., Langlois, C., Munschauer, M., Dewell, S., Hafner, M., et al. (2012). FMRP targets distinct mRNA sequence elements to regulate protein expression. Nature *492*, 382–386.

Bear, M.F., Huber, K.M., and Warren, S.T. (2004). The mGluR theory of fragile X mental retardation. Trends Neurosci. *27*, 370–377.

Bernt, K.M., Zhu, N., Sinha, A.U., Vempati, S., Faber, J., Krivtsov, A.V., Feng, Z., Punt, N., Daigle, A., Bullinger, L., et al. (2011). MLL-rearranged leukemia is dependent on aberrant H3K79 methylation by DOT1L. Cancer Cell *20*, 66–78.

Blonden, L., van 't Padje, S., Severijnen, L.A., Destree, O., Oostra, B.A., and Willemsen, R. (2005). Two members of the Fxr gene family, Fmr1 and Fxr1, are differentially expressed in Xenopus tropicalis. Int. J. Dev. Biol. *49*, 437–441.

Brown, E.J., and Baltimore, D. (2003). Essential and dispensable roles of ATR in cell cycle arrest and genome maintenance. Genes Dev. *17*, 615–628.

Cabart, P., Chew, H.K., and Murphy, S. (2004). BRCA1 cooperates with NUFIP and P-TEFb to activate transcription by RNA polymerase II. Oncogene *23*, 5316–5329.

Celeste, A., Petersen, S., Romanienko, P.J., Fernandez-Capetillo, O., Chen, H.T., Sedelnikova, O.A., Reina-San-Martin, B., Coppola, V., Meffre, E., Difilippantonio, M.J., et al. (2002). Genomic instability in mice lacking histone H2AX. Science *296*, 922–927.

Ciccia, A., and Elledge, S.J. (2010). The DNA damage response: making it safe to play with knives. Mol. Cell *40*, 179–204.

Collins, S.C., Bray, S.M., Suhl, J.A., Cutler, D.J., Coffee, B., Zwick, M.E., and Warren, S.T. (2010). Identification of novel FMR1 variants by massively parallel sequencing in developmentally delayed males. Am. J. Med. Genet. A. *152A*, 2512–2520.

Deng, P.Y., Rotman, Z., Blundon, J.A., Cho, Y., Cui, J., Cavalli, V., Zakharenko, S.S., and Klyachko, V.A. (2013). FMRP regulates neurotransmitter release and synaptic information transmission by modulating action potential duration via BK channels. Neuron *77*, 696–711.

Downs, J.A., Nussenzweig, M.C., and Nussenzweig, A. (2007). Chromatin dynamics and the preservation of genetic information. Nature *447*, 951–958.

Feng, Y., Gutekunst, C.A., Eberhart, D.E., Yi, H., Warren, S.T., and Hersch, S.M. (1997). Fragile X mental retardation protein: nucleocytoplasmic shuttling and association with somatodendritic ribosomes. J. Neurosci. *17*, 1539–1547.

Fraune, J., Schramm, S., Alsheimer, M., and Benavente, R. (2012). The mammalian synaptonemal complex: protein components, assembly and role in meiotic recombination. Exp. Cell Res. *318*, 1340–1346.

Garcia-Cruz, R., Roig, I., Robles, P., Scherthan, H., and Garcia Caldés, M. (2009). ATR, BRCA1 and gammaH2AX localize to unsynapsed chromosomes at the pachytene stage in human oocytes. Reprod. Biomed. Online *18*, 37–44.

Isabelle, M., Moreel, X., Gagné, J.P., Rouleau, M., Ethier, C., Gagné, P., Hendzel, M.J., and Poirier, G.G. (2010). Investigation of PARP-1, PARP-2, and PARG interactomes by affinity-purification mass spectrometry. Proteome Sci. *8*, 22.

Jenkins, E.C., Tassone, F., Ye, L., Gu, H., Xi, M., Velinov, M., Brown, W.T., Hagerman, R.J., and Hagerman, P.J. (2008). Reduced telomere length in older men with premutation alleles of the fragile X mental retardation 1 gene. Am. J. Med. Genet. A. *146A*, 1543–1546.

Jeon, S.J., Seo, J.E., Yang, S.I., Choi, J.W., Wells, D., Shin, C.Y., and Ko, K.H. (2011). Cellular stress-induced up-regulation of FMRP promotes cell survival by modulating PI3K-Akt phosphorylation cascades. J. Biomed. Sci. *18*, 17.

Jeon, S.J., Han, S.H., Yang, S.I., Choi, J.W., Kwon, K.J., Park, S.H., Kim, H.Y., Cheong, J.H., Ryu, J.H., Ko, K.H., et al. (2012). Positive feedback regulation of Akt-FMRP pathway protects neurons from cell death. J. Neurochem. *123*, 226–238.

Johannisson, R., Rehder, H., Wendt, V., and Schwinger, E. (1987). Spermatogenesis in two patients with the fragile X syndrome. I. Histology: light and electron microscopy. Hum. Genet. *76*, 141–147.

Kim, M., Bellini, M., and Ceman, S. (2009). Fragile X mental retardation protein FMRP binds mRNAs in the nucleus. Mol. Cell. Biol. *29*, 214–228.

Kwan, K.Y., Moens, P.B., and Wang, J.C. (2003). Infertility and aneuploidy in mice lacking a type IA DNA topoisomerase III beta. Proc. Natl. Acad. Sci. USA *100*, 2526–2531.

Liu, W., Jiang, F., Bi, X., and Zhang, Y.Q. (2012). Drosophila FMRP participates in the DNA damage response by regulating G2/M cell cycle checkpoint and apoptosis. Hum. Mol. Genet. *21*, 4655–4668.

Lucá, R., Averna, M., Zalfa, F., Vecchi, M., Bianchi, F., La Fata, G., Del Nonno, F., Nardacci, R., Bianchi, M., Nuciforo, P., et al. (2013). The fragile X protein binds mRNAs involved in cancer progression and modulates metastasis formation. EMBO Mol. Med. *5*, 1523–1536.

Malter, H.E., Iber, J.C., Willemsen, R., de Graaff, E., Tarleton, J.C., Leisti, J., Warren, S.T., and Oostra, B.A. (1997). Characterization of the full fragile X syndrome mutation in fetal gametes. Nat. Genet. *15*, 165–169.

Maurer-Stroh, S., Dickens, N.J., Hughes-Davies, L., Kouzarides, T., Eisenhaber, F., and Ponting, C.P. (2003). The Tudor domain 'Royal Family': Tudor, plant Agenet, Chromo, PWWP and MBT domains. Trends Biochem. Sci. *28*, 69–74.

Nagaraju, G., and Scully, R. (2007). Minding the gap: the underground functions of BRCA1 and BRCA2 at stalled replication forks. DNA Repair (Amst.) *6*, 1018–1031.

Nelson, D.L. (1995). The fragile X syndromes. Semin. Cell Biol. *6*, 5–11.

O'Donnell, W.T., and Warren, S.T. (2002). A decade of molecular studies of fragile X syndrome. Annu. Rev. Neurosci. *25*, 315–338.

Ontoso, D., Acosta, I., van Leeuwen, F., Freire, R., and San-Segundo, P.A. (2013). Dot1-dependent histone H3K79 methylation promotes activation of the Mek1 meiotic checkpoint effector kinase by regulating the Hop1 adaptor. PLoS Genet. *9*, e1003262.

Ontoso, D., Kauppi, L., Keeney, S., and San-Segundo, P.A. (2014). Dynamics of DOT1L localization and H3K79 methylation during meiotic prophase I in mouse spermatocytes. Chromosoma *123*, 147–164.

Ramos, A., Hollingworth, D., Adinolfi, S., Castets, M., Kelly, G., Frenkiel, T.A., Bardoni, B., and Pastore, A. (2006). The structure of the N-terminal domain of the fragile X mental retardation protein: a platform for protein-protein interaction. Structure *14*, 21–31.

Reeve, S.P., Bassetto, L., Genova, G.K., Kleyner, Y., Leyssen, M., Jackson, F.R., and Hassan, B.A. (2005). The Drosophila fragile X mental retardation protein controls actin dynamics by directly regulating profilin in the brain. Curr. Biol. *15*, 1156–1163.

Reyniers, E., Vits, L., De Boulle, K., Van Roy, B., Van Velzen, D., de Graaff, E., Verkerk, A.J., Jorens, H.Z., Darby, J.K., Oostra, B., et al. (1993). The full mutation in the FMR-1 gene of male fragile X patients is absent in their sperm. Nat. Genet. *4*, 143–146.

Sabra, M., Texier, P., El Maalouf, J., and Lomonte, P. (2013). The Tudor protein survival motor neuron (SMN) is a chromatin-binding protein that interacts with methylated lysine 79 of histone H3. J. Cell Sci. *126*, 3664–3677.

Santoro, M.R., Bray, S.M., and Warren, S.T. (2012). Molecular mechanisms of fragile X syndrome: a twenty-year perspective. Annu. Rev. Pathol. *7*, 219–245.

Schultz-Pedersen, S., Hasle, H., Olsen, J.H., and Friedrich, U. (2001). Evidence of decreased risk of cancer in individuals with fragile X. Am. J. Med. Genet. *103*, 226–230.

Tamanini, F., Bontekoe, C., Bakker, C.E., van Unen, L., Anar, B., Willemsen, R., Yoshida, M., Galjaard, H., Oostra, B.A., and Hoogeveen, A.T. (1999). Different targets for the fragile X-related proteins revealed by their distinct nuclear localizations. Hum. Mol. Genet. *8*, 863–869.

Tian, H., Cao, Y.X., Zhang, X.S., Liao, W.P., Yi, Y.H., Lian, J., Liu, L., Huang, H.L., Liu, W.J., Yin, M.M., et al. (2013). The targeting and functions of miRNA-383 are mediated by FMRP during spermatogenesis. Cell Death Dis. *4*, e617.

Turner, G., Daniel, A., and Frost, M. (1980). X-linked mental retardation, macroorchidism, and the Xq27 fragile site. J. Pediatr. *96*, 837–841.

Wolffe, A.P., and Guschin, D. (2000). Review: chromatin structural features and targets that regulate transcription. J. Struct. Biol. *129*, 102–122.

Zhou, B.B., and Elledge, S.J. (2000). The DNA damage response: putting checkpoints in perspective. Nature *408*, 433–439.

EXTENDED EXPERIMENTAL PROCEDURES

Chemicals

Aphidicolin (Sigma), hydroxyurea (Sigma), leptomycin B (Sigma).

Cells and Cell Culture

Cells were grown in DMEM media (GIBCO) supplemented with 10% FBS, 2 mM L-Glutamine, 100 units/ml Penicillin, and 100 μg/ml Streptomycin.

MEFs

FMRP KO MEFs were created with an insertion in exon 5 resulting in FMRP protein null MEFs with low level of FMRP mRNA (The Dutch-Belgian Fragile X Consortium, 1994). DOT1L mutant MEFs, which have a significant reduction in H3K79 methylation levels, were created using a gene trap approach (Steger et al., 2008).

Antibodies

Mouse anti-FMRP (Chemicon, MAB2160), rabbit anti-FMRP (Abcam, ab17722), rabbit anti-H3 (Abcam), mouse anti-H2A.X phosphorylated on Ser 139 (anti-γH2A.X) (Abcam), mouse anti-H2A.X phosphorylated on Ser 139 (anti-γH2A.X) (Millipore), rabbit anti-H2A.X (Abcam), mouse anti-Actin (Abcam), goat anti-ATR (Santa Cruz), rabbit anti-BRCA1 (Bethyl), rabbit anti-mouse BRCA1 (gift of S. Namekawa), rabbit anti-phospho-BRCA1(Ser1423) (Abcam), rabbit anti-phospho-BRCA1(Ser1423) (Mybiosource) (recognizes mouse epitope), rabbit anti-RPA32 (Bethyl), mouse anti-CENTB (Santa Cruz), mouse anti-SYCP3 (Santa Cruz), rabbit anti-SYCP1 (Abcam), goat anti-SYCP1 (Santa Cruz), rabbit anti-DMC1 (Santa Cruz), mouse anti-MLH1 (Millipore), mouse anti-SPO11. Anti-SPO11 hybridoma cell line 180 was generated by M.P. Thelen at Lawrence Livermore National Laboratory, California; the purified monoclonal antibody was provided by S. Keeney, Memorial Sloan-Kettering Cancer Center, New York.

Western Blot Band Intensity Quantification

For western blot quantification we measured band intensity using ImageJ software. In the case of BRCA1 phosphorylation we used Photoshop software. For γH2A.X induction we quantified the γH2A.X band in the "treatment" lane and then compared the value to control treatment, e.g., DMSO or the 0 time point.

Histone MLA Binding Reactions

The binding reactions were performed in binding buffer (50 mM Tris pH 7.5, 1 M NaCl, 2 mM $MgCl_2$, 0.5% Triton X-100) at +4C° for 1 hr with rotation. After incubation with glutathione agarose beads (GE Healthcare) the reactions were washed 5 times with binding buffer.

Calculation of Chromatin-Associated FMRP

In quantification of FMRP chromatin recruitment, the y axis represents the ratio of chromatin-associated FMRP to total FMRP. It was calculated based on the level of FMRP on chromatin divided by total FMRP. The data are from 3 independent experiments. The relative fold increase in FMRP loading on chromatin in response to aphidicolin (APH) is compared to the levels of chromatin-associated FMRP upon DMSO treatment, which was designated as 1 (DMSO).

Aphidicolin Treatment

APH treatment was performed for 24 hr.

γH2A.X Analysis in MEF Cells after Replication Inhibition by Aphidicolin

MEFs were treated with DMSO or APH (0.5μM) for 24 hr. Cells were then lysed in SDS loading buffer and samples were subjected to western analysis for γH2A.X and total H2A.X. Three independent experiments were performed.

pS1423 BRCA1 Analysis after Replication Inhibition by Aphidicolin

For HeLa cells, the APH treatment was 0.5μM for 24 hr. For 293 and MEF cells, the treatment was 5μM for 24 hr. Cells were then lysed in SDS loading buffer and samples were subjected to western analysis for pS1423 BRCA1 and total BRCA1. The quantification was performed as a ratio of phospho-BRCA1 to total BRCA1. Three independent experiments were performed.

FMRP RNAi Analysis in HeLa Cells and Treatment with Aphidicolin for γH2A.X Induction

HeLa cells were transfected with two different FMRP shRNA constructs (FMRP shRNA1 and FMRP shRNA2) or control scramble shRNA. After 3 days cells were treated with DMSO or aphidicolin (0.5μM) for 24 hr. Cells were then lysed in SDS sample buffer and subjected to western blot using FMRP, actin, γH2A.X, and H2A.X antibodies. Three independent experiments were performed.

Hydroxyurea Treatment Experiments

MEFs were treated with DMSO or hydroxyurea at 2 mM final concentration and incubated for 0, 30, 60, and 120 min. Cells were then lysed in SDS sample buffer and samples were analyzed by western blotting using γH2A.X antibody and H2A.X antibody. Three independent experiments were performed.

UV Irradiation

MEF cells were UV irradiated with a dose of 50 J/m^2 and cell samples were collected 0, 30, 60, and 120 min postirradiation in SDS sample buffer. Samples were then western blotted for γH2A.X and H2A.X. Three independent experiments were performed.

Ionizing Radiation Treatment

MEFs were treated with 5Gy of ionizing radiation and samples were collected in SDS loading buffer 30 min postirradiation. Western blots were performed using γH2A.X and H2A.X antibodies. Experiments were performed 3 times.

Colony Survival Assay

For the colony survival assays we used HeLa cells stably expressing FMRP RNAi vector, which were complemented with stably expressing rescue vector, either wild-type FMRP-Flag-HA or Flag-HA alone. Cells were seeded at 200 cells/dish density and allowed to attach. The media was then changed to aphidicolin (APH) containing media (0.05μM, 0.1μM, and 0.3μM) or control media containing DMSO. Cells were incubated for 2 weeks until the appearance of colonies. The colonies were then rinsed in PBS, fixed in methanol and stained with Coomassie stain. Survival was determined by comparing the amount of colonies in APH containing media to the number of colonies in control media. Statistical analysis of data from 3 independent experiments was done using 2-way ANOVA. For MEF cells, the protocol was the same except that the cells were treated with 0.01μM or 0.05μM of APH, or 0.01 or 0.03 mM of hydroxyurea (HU).

Lentivirus Production

Lentiviral particles were produced as previously described (Lois et al., 2002). Briefly, HEK293FT cells were transfected using the calcium phosphate method with FIV-CMV-pEGFP-FMRP (gift, G.J. Bassel, Emory University) and packaging vectors. The supernatants containing the viral particles were collected 48 hr after transfection and concentrated using ultracentrifugation. Viral titers were determined by serial dilution of HEK293FT cells as 10^8 per ml. Primary cell cultures were transduced by adding concentrated lentivirus to the growth media.

Hippocampal Neuron Cell Culture and Infection

Hippocampal primary neurons were dissected from WT and *Fmr1* KO mice at embryonic day 16.5 and cultured as described previously (Bassell and Warren, 2008) in accordance with the Institutional Animal Care and Use Committee guidelines. Cells were plated (2000 cells per cm^2) on poly-l-lysine-coated Biotechs coverslips (1 mg/ml) in MEM with FBS (10%) for 2 hr, supplemented with B-27 and Gluta MAX-1 (Invitrogen, San Diego, CA). Neurons were transduced with lentivirus at 14 days in vitro (DIV). Six hours posttransduction, live neurons were processed for the AMPAR internalization assay. FMRP KO MEFs were reconstituted with FMRP-Flag-HA constructs using pMSCV-based viral vector system.

Constitutive AMPAR Internalization Assay

The assay was performed as described previously for rat neurons (Nakamoto et al., 2007) with modifications (Bhattacharyya et al., 2009). Surface AMPARs in live *Fmr1* knockout mouse neurons were labeled with a rabbit polyclonal antibody against the N terminus of the GluR1 subunit (Calbiochem, 1:5 in conditioned media) for 15 min at 37°C, 0.5% CO_2. After incubation with antagonists (1 μM TTX, 10 μM NBQX, and 50 μM APV; Tocris) in conditioned media for 15 min at 37°C, 0.5% CO_2, cells were fixed in 4% FA for 15 min on ice, and labeled surface GluR1s were visualized by saturating with Alexa 546 conjugated goat-anti-rabbit secondary antibody (Invitrogen). After permeabilization with 0.1% Triton X-100 for 30 min at room temperature, internalized GluR1s were saturated with Alexa 633-conjugated donkey anti-rabbit secondary antibody. Raw images were taken with a Zeiss confocal microscope and LSM software, and were compared between samples in the same culture preparation. Signal in identical areas of thick distal dendrites (>20 μm from the soma) were measured. p values were determined using one-way ANOVA ($\alpha = 0.05$) with Bonferroni's post hoc test.

Microscale Thermophoresis from Nanotemper Technologies

The process involves measurement of the fluorescence distribution of fluorescently labeled molecules inside a capillary upon laser irradiation. A temperature gradient is generated by an IR-Laser focused into the capillary. Binding affinities are calculating measuring a temperature jump in the initial stage of irradiation, thermophoretic movement of the molecules within the gradient at later stages, or both (Jerabek-Willemsen et al., 2011; Wienken et al., 2010). Independent experiments were performed a minimum of 3 times for each histone modification. In MST experiments using MLA histones, the Agenet domain was labeled. Histone MLAs were prepared as described (Simon et al., 2007) and purchased from Active Motif. Histone binding reactions with the Agenet domain were performed in binding buffer (50 mM Tris pH 7.5, 1 M NaCl, 2 mM $MgCl_2$, 0.5% Triton X-100) at room temperature for 30 min. In the case of the nucleosome MST reaction recombinant H3K79me2 nucleosome was labeled. Mononucleosomes were prepared as described (Lu

et al., 2008), and incubation in binding buffer (50 mM Tris pH 7.5, 150 mM NaCl, 2 mM $MgCl_2$, 0.5% Triton X-100) was for 3 hr at room temperature. Data were plotted using GraphPad Prizm software.

Fmr1 KO Mice

Fmr1 KO mice (allele tm1^{Cgr}/J, congenic on a C57BL/6J background; same mutation as used for *Fmr1* KO MEFs) were a kind gift from Mark Bear. Mice were kept under standard conditions and all experiments were conducted in compliance with the Animal Welfare act and approved by the Animal Care and Use Committee at the appropriate institution.

Dot1L cKO Mice

Dot1L$^{fl/fl}$ conditional KO mice were a kind gift from Scott Armstrong. To generate a germ-cell-specific *Dot1L* deletion, a germline-specific *Cre* transgene (*Mvh-Cre*, [Hu et al., 2013]) was crossed into the *Dot1L*^{fl} background. *Mvh-Cre;Dot1L*$^{fl/+}$ male mice (germ cell genotype *Dot1L*$^{\Delta/+}$) were mated to *Dot1L*$^{fl/fl}$ females, so that F_1 males were either *Dot1L*$^{fl/\Delta}$ or *Dot1L*$^{fl/+}$. Conditional KO (cKO) animals were *Cre*-positive *Dot1L*$^{fl/\Delta}$ males (germ cell genotype *Dot1L* $^{\Delta/\Delta}$), and *Cre*-negative *Dot1L*$^{fl/+}$ males were used as littermate controls.

SUPPLEMENTAL REFERENCES

Bächner, D., Manca, A., Steinbach, P., Wöhrle, D., Just, W., Vogel, W., Hameister, H., and Poustka, A. (1993). Enhanced expression of the murine FMR1 gene during germ cell proliferation suggests a special function in both the male and the female gonad. Hum. Mol. Genet. *2*, 2043–2050.

Bassell, G.J., and Warren, S.T. (2008). Fragile X syndrome: loss of local mRNA regulation alters synaptic development and function. Neuron *60*, 201–214.

Bhattacharyya, S., Biou, V., Xu, W., Schlüter, O., and Malenka, R.C. (2009). A critical role for PSD-95/AKAP interactions in endocytosis of synaptic AMPA receptors. Nat. Neurosci. *12*, 172–181.

Bishop, D.K., Park, D., Xu, L., and Kleckner, N. (1992). DMC1: a meiosis-specific yeast homolog of E. coli recA required for recombination, synaptonemal complex formation, and cell cycle progression. Cell *69*, 439–456.

Blanco-Rodríguez, J. (2012). Programmed phosphorylation of histone H2AX precedes a phase of DNA double-strand break-independent synapsis in mouse meiosis. Reproduction *144*, 699–712.

Bostelman, L.J., Keller, A.M., Albrecht, A.M., Arat, A., and Thompson, J.S. (2007). Methylation of histone H3 lysine-79 by Dot1p plays multiple roles in the response to UV damage in Saccharomyces cerevisiae. DNA Repair (Amst.) *6*, 383–395.

Brown, V., Jin, P., Ceman, S., Darnell, J.C., O'Donnell, W.T., Tenenbaum, S.A., Jin, X., Feng, Y., Wilkinson, K.D., Keene, J.D., et al. (2001). Microarray identification of FMRP-associated brain mRNAs and altered mRNA translational profiles in fragile X syndrome. Cell *107*, 477–487.

Conde, F., Refolio, E., Cordón-Preciado, V., Cortés-Ledesma, F., Aragón, L., Aguilera, A., and San-Segundo, P.A. (2009). The Dot1 histone methyltransferase and the Rad9 checkpoint adaptor contribute to cohesin-dependent double-strand break repair by sister chromatid recombination in Saccharomyces cerevisiae. Genetics *182*, 437–446.

Costelloe, T., Fitzgerald, J., Murphy, N.J., Flaus, A., and Lowndes, N.F. (2006). Chromatin modulation and the DNA damage response. Exp. Cell Res. *312*, 2677–2686.

Gagné, J.P., Bonicalzi, M.E., Gagné, P., Ouellet, M.E., Hendzel, M.J., and Poirier, G.G. (2005). Poly(ADP-ribose) glycohydrolase is a component of the FMRP-associated messenger ribonucleoparticles. Biochem. J. *392*, 499–509.

Garber, K.B., Visootsak, J., and Warren, S.T. (2008). Fragile X syndrome. Eur. J. Hum. Genet. *16*, 666–672.

Gatei, M., Zhou, B.B., Hobson, K., Scott, S., Young, D., and Khanna, K.K. (2001). Ataxia telangiectasia mutated (ATM) kinase and ATM and Rad3 related kinase mediate phosphorylation of Brca1 at distinct and overlapping sites. In vivo assessment using phospho-specific antibodies. J. Biol. Chem. *276*, 17276–17280.

Haince, J.F., Kozlov, S., Dawson, V.L., Dawson, T.M., Hendzel, M.J., Lavin, M.F., and Poirier, G.G. (2007). Ataxia telangiectasia mutated (ATM) signaling network is modulated by a novel poly(ADP-ribose)-dependent pathway in the early response to DNA-damaging agents. J. Biol. Chem. *282*, 16441–16453.

Handel, M.A., and Schimenti, J.C. (2010). Genetics of mammalian meiosis: regulation, dynamics and impact on fertility. Nat. Rev. Genet. *11*, 124–136.

Helleday, T., Bryant, H.E., and Schultz, N. (2005). Poly(ADP-ribose) polymerase (PARP-1) in homologous recombination and as a target for cancer therapy. Cell Cycle *4*, 1176–1178.

Hu, Y.C., de Rooij, D.G., and Page, D.C. (2013). Tumor suppressor gene Rb is required for self-renewal of spermatogonial stem cells in mice. Proc. Natl. Acad. Sci. USA *110*, 12685–12690.

Jerabek-Willemsen, M., Wienken, C.J., Braun, D., Baaske, P., and Duhr, S. (2011). Molecular interaction studies using microscale thermophoresis. Assay Drug Dev. Technol. *9*, 342–353.

Kedar, P.S., Stefanick, D.F., Horton, J.K., and Wilson, S.H. (2008). Interaction between PARP-1 and ATR in mouse fibroblasts is blocked by PARP inhibition. DNA Repair (Amst.) *7*, 1787–1798.

Krum, S.A., la Rosa Dalugdugan, Ed., Miranda-Carboni, G.A., and Lane, T.F. (2010). BRCA1 forms a functional complex with γ-H2AX as a late response to genotoxic stress. J. Nucleic Acids *2010*, pii: 801594.

Liu, S., Bekker-Jensen, S., Mailand, N., Lukas, C., Bartek, J., and Lukas, J. (2006). Claspin operates downstream of TopBP1 to direct ATR signaling towards Chk1 activation. Mol. Cell. Biol. *26*, 6056–6064.

Lois, C., Hong, E.J., Pease, S., Brown, E.J., and Baltimore, D. (2002). Germline transmission and tissue-specific expression of transgenes delivered by lentiviral vectors. Science *295*, 868–872.

Lu, X., Simon, M.D., Chodaparambil, J.V., Hansen, J.C., Shokat, K.M., and Luger, K. (2008). The effect of H3K79 dimethylation and H4K20 trimethylation on nucleosome and chromatin structure. Nat. Struct. Mol. Biol. *15*, 1122–1124.

Méndez, J., and Stillman, B. (2000). Chromatin association of human origin recognition complex, cdc6, and minichromosome maintenance proteins during the cell cycle: assembly of prereplication complexes in late mitosis. Mol. Cell. Biol. *20*, 8602–8612.

Moens, P.B., Kolas, N.K., Tarsounas, M., Marcon, E., Cohen, P.E., and Spyropoulos, B. (2002). The time course and chromosomal localization of recombination-related proteins at meiosis in the mouse are compatible with models that can resolve the early DNA-DNA interactions without reciprocal recombination. J. Cell Sci. *115*, 1611–1622.

Nakamoto, M., Nalavadi, V., Epstein, M.P., Narayanan, U., Bassell, G.J., and Warren, S.T. (2007). Fragile X mental retardation protein deficiency leads to excessive mGluR5-dependent internalization of AMPA receptors. Proc. Natl. Acad. Sci. USA *104*, 15537–15542.

Pei, H., Zhang, L., Luo, K., Qin, Y., Chesi, M., Fei, F., Bergsagel, P.L., Wang, L., You, Z., and Lou, Z. (2011). MMSET regulates histone H4K20 methylation and 53BP1 accumulation at DNA damage sites. Nature *470*, 124–128.

Peters, A.H., Plug, A.W., van Vugt, M.J., and de Boer, P. (1997). A drying-down technique for the spreading of mammalian meiocytes from the male and female germline. Chromosome Res. *5*, 66–68.

Pittman, D.L., Cobb, J., Schimenti, K.J., Wilson, L.A., Cooper, D.M., Brignull, E., Handel, M.A., and Schimenti, J.C. (1998). Meiotic prophase arrest with failure of chromosome synapsis in mice deficient for Dmc1, a germline-specific RecA homolog. Mol. Cell *1*, 697–705.

Rogakou, E.P., Pilch, D.R., Orr, A.H., Ivanova, V.S., and Bonner, W.M. (1998). DNA double-stranded breaks induce histone H2AX phosphorylation on serine 139. J. Biol. Chem. *273*, 5858–5868.

San-Segundo, P.A., and Roeder, G.S. (2000). Role for the silencing protein Dot1 in meiotic checkpoint control. Mol. Biol. Cell *11*, 3601–3615.

Schwacha, A., and Kleckner, N. (1997). Interhomolog bias during meiotic recombination: meiotic functions promote a highly differentiated interhomolog-only pathway. Cell *90*, 1123–1135.

Simon, M.D., Chu, F., Racki, L.R., de la Cruz, C.C., Burlingame, A.L., Panning, B., Narlikar, G.J., and Shokat, K.M. (2007). The site-specific installation of methyllysine analogs into recombinant histones. Cell *128*, 1003–1012.

Slegtenhorst-Eegdeman, K.E., de Rooij, D.G., Verhoef-Post, M., van de Kant, H.J., Bakker, C.E., Oostra, B.A., Grootegoed, J.A., and Themmen, A.P. (1998). Macroorchidism in FMR1 knockout mice is caused by increased Sertoli cell proliferation during testicular development. Endocrinology *139*, 156–162.

Steger, D.J., Lefterova, M.I., Ying, L., Stonestrom, A.J., Schupp, M., Zhuo, D., Vakoc, A.L., Kim, J.E., Chen, J., Lazar, M.A., et al. (2008). DOT1L/KMT4 recruitment and H3K79 methylation are ubiquitously coupled with gene transcription in mammalian cells. Mol. Cell. Biol. *28*, 2825–2839.

Stoll, G., Pietiläinen, O.P., Linder, B., Suvisaari, J., Brosi, C., Hennah, W., Leppä, V., Torniainen, M., Ripatti, S., Ala-Mello, S., et al. (2013). Deletion of TOP3β, a component of FMRP-containing mRNPs, contributes to neurodevelopmental disorders. Nat. Neurosci. *16*, 1228–1237.

Stucki, M., and Jackson, S.P. (2006). gammaH2AX and MDC1: anchoring the DNA-damage-response machinery to broken chromosomes. DNA Repair (Amst.) *5*, 534–543.

The Dutch-Belgian Fragile X Consortium (1994). Fmr1 knockout mice: a model to study fragile X mental retardation. Cell *78*, 23–33.

Tibbetts, R.S., Cortez, D., Brumbaugh, K.M., Scully, R., Livingston, D., Elledge, S.J., and Abraham, R.T. (2000). Functional interactions between BRCA1 and the checkpoint kinase ATR during genotoxic stress. Genes Dev. *14*, 2989–3002.

Turner, G., Eastman, C., Casey, J., McLeay, A., Procopis, P., and Turner, B. (1975). X-linked mental retardation associated with macro-orchidism. J. Med. Genet. *12*, 367–371.

Turner, J.M., Aprelikova, O., Xu, X., Wang, R., Kim, S., Chandramouli, G.V., Barrett, J.C., Burgoyne, P.S., and Deng, C.X. (2004). BRCA1, histone H2AX phosphorylation, and male meiotic sex chromosome inactivation. Curr. Biol. *14*, 2135–2142.

Turner, J.M., Mahadevaiah, S.K., Fernandez-Capetillo, O., Nussenzweig, A., Xu, X., Deng, C.X., and Burgoyne, P.S. (2005). Silencing of unsynapsed meiotic chromosomes in the mouse. Nat. Genet. *37*, 41–47.

van 't Padje, S., Engels, B., Blonden, L., Severijnen, L.A., Verheijen, F., Oostra, B.A., and Willemsen, R. (2005). Characterisation of Fmrp in zebrafish: evolutionary dynamics of the fmr1 gene. Dev. Genes Evol. *215*, 198–206.

Wakeman, T.P., Wang, Q., Feng, J., and Wang, X.F. (2012). Bat3 facilitates H3K79 dimethylation by DOT1L and promotes DNA damage-induced 53BP1 foci at G1/G2 cell-cycle phases. EMBO J. *31*, 2169–2181.

Ward, I.M., and Chen, J. (2001). Histone H2AX is phosphorylated in an ATR-dependent manner in response to replicational stress. J. Biol. Chem. *276*, 47759–47762.

Warren, S.T., and Nelson, D.L. (1994). Advances in molecular analysis of fragile X syndrome. JAMA *271*, 536–542.

Wienken, C.J., Baaske, P., Rothbauer, U., Braun, D., and Duhr, S. (2010). Protein-binding assays in biological liquids using microscale thermophoresis. Nat. Commun. *1*, 100.

Wysocki, R., Javaheri, A., Allard, S., Sha, F., Côté, J., and Kron, S.J. (2005). Role of Dot1-dependent histone H3 methylation in G1 and S phase DNA damage checkpoint functions of Rad9. Mol. Cell. Biol. *25*, 8430–8443.

Yoshida, K., Kondoh, G., Matsuda, Y., Habu, T., Nishimune, Y., and Morita, T. (1998). The mouse RecA-like gene Dmc1 is required for homologous chromosome synapsis during meiosis. Mol. Cell *1*, 707–718.

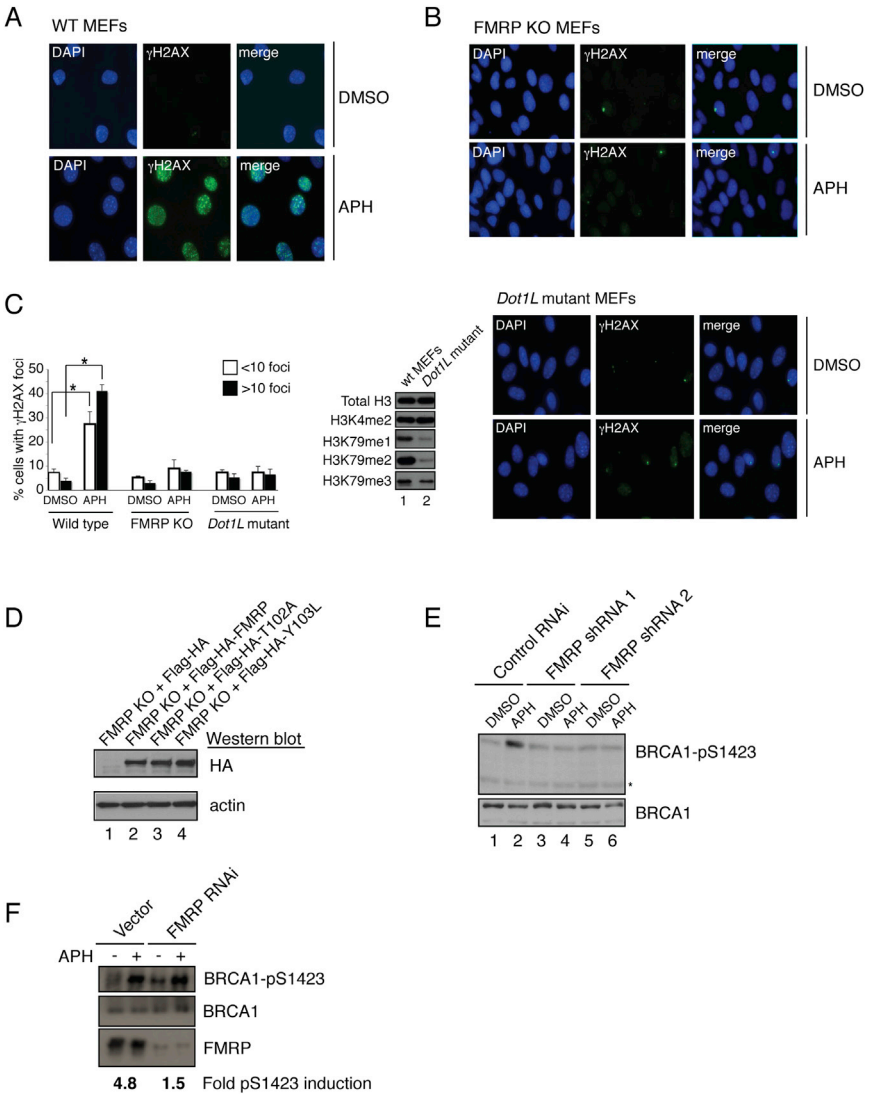

Figure S1. FMRP-Mediated γH2A.X Induction and BRCA1 Phosphorylation, Related to Figures 1, 3, and 7

(A and B) Induction of γH2A.X foci formation is impaired in FMRP KO (B) as compared to wild-type MEFs (A) in response to aphidicolin (APH) treatment.

(C) Left graph, wild-type but not FMRP KO and *Dot1L* mutant MEFs exhibited a 3-fold (cells with < 10 foci) and 4-fold (cells with > 10 foci) increase in γH2A.X foci in response to APH. Asterisks, $p < 0.05$, Student t test. Data are represented as average of three independent experiments with SD. Western blot shows H3K79 methylation levels in WT and *Dot1L* mutant MEFs. Right: induction of γH2A.X foci formation in response to APH is impaired in *Dot1L* mutant MEFs as compared to wild-type MEFs (A).

(D) Western blot showing the levels of expression of exogenous Flag-HA-FMRP (lane 2) and FMRP Agenet domain mutants (lanes 3 and 4) in FMRP KO MEFs.

(E) HeLa cells were subjected to scrambled or two independent FMRP shRNAs (FMRP shRNA1 and FMRP shRNA2). Cells were then treated with DMSO as a control or APH for 24 hr, followed by western blotting for BRCA1 phospho-Ser1423. In contrast to control RNAi cells (3.5-fold induction in Ser1423 phosphorylation), FMRP RNAi cells showed no phosphorylation of BRCA1 at Ser1423 in response to APH treatment (compare lane 2 to 4 and 6). Asterisk indicates a nonspecific band.

(F) Unlike in HeLa cells, in 293 cells FMRP RNAi-mediated dampening of phospho-Ser1423 could be partially attributed to the increased levels of phospho-Ser1423 even in the absence of APH treatment, suggesting that the FMRP effect on BRCA1 phosphorylation might be context dependent. Blots are representative of three experiments.

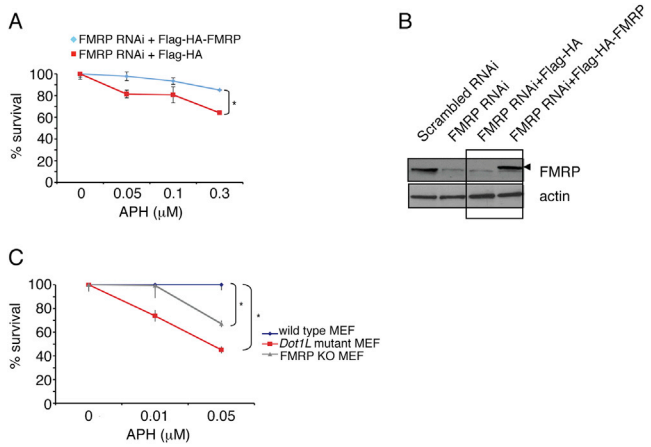

Figure S2. FMRP and DOT1L-Dependent Cell Survival Assays, Related to Figures 1 and 7

(A) HeLa cells stably expressing an FMRP RNAi hairpin and reconstituted with an RNAi resistant wild-type FMRP-Flag-HA construct or empty Flag-HA vector. FMRP RNAi+Flag-HA cells exhibited more cell death (asterisks $p < 0.05$, $n = 3$, 2-way ANOVA) in response to the increased concentration of APH as compared to FMRP RNAi+FMRP-Flag-HA cells.

(B) FMRP levels in cells used for the colony survival assays are shown in the box. Scrambled RNAi and FMRP RNAi are shown for comparison. Arrowhead demarcates exogenous Flag-HA-FMRP.

(C) Colony survival assays in the presence of APH using wild-type MEFs, FMRP KO MEFs and *Dot1L* mutant MEFs. FMRP KO MEFs and *Dot1L* mutant MEFs were more sensitive to the increased concentrations of APH as compared to wild-type MEFs (asterisks $p < 0.05$, $n = 3$, 2-way ANOVA).

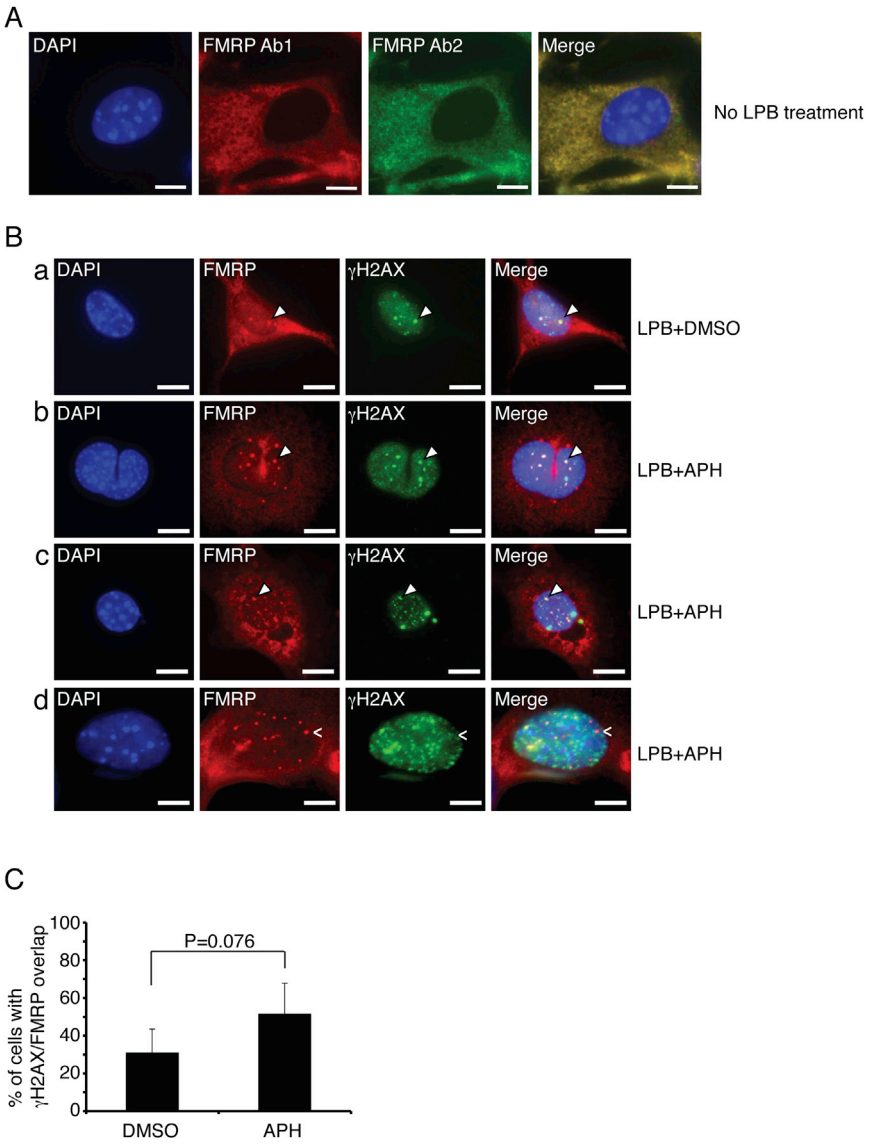

Figure S3. FMRP and γH2A.X Colocalization, Related to Figure 2

(A) FMRP immunostaining with anti-FMRP antibody (1) (Abcam, red) and a second anti-FMRP antibody (2) (Calbiochem, green) without leptomycin B (LPB) treatment, indicating low levels of nuclear FMRP. Scale bar, 10 μm.

(B) Overlap of FMRP and γH2A.X foci in the presence of leptomycin B (LPB) in DMSO or APH treated MEFs. a,b,c show various degrees of γH2A.X/FMRP overlap indicated by solid arrowheads. d shows an example of a cell where FMRP and γH2A.X do not overlap (arrowhead). Scale bar, 10 μm.

(C) Graph shows that about 30% of cells displayed at least partial (at least 1 overlap event per cell) γH2A.X/FMRP overlap, which was increased upon APH treatment, although it was not a statistically significant increase ($p = 0.076$, Student t test). Data are represented as average of three independent experiments with SD.

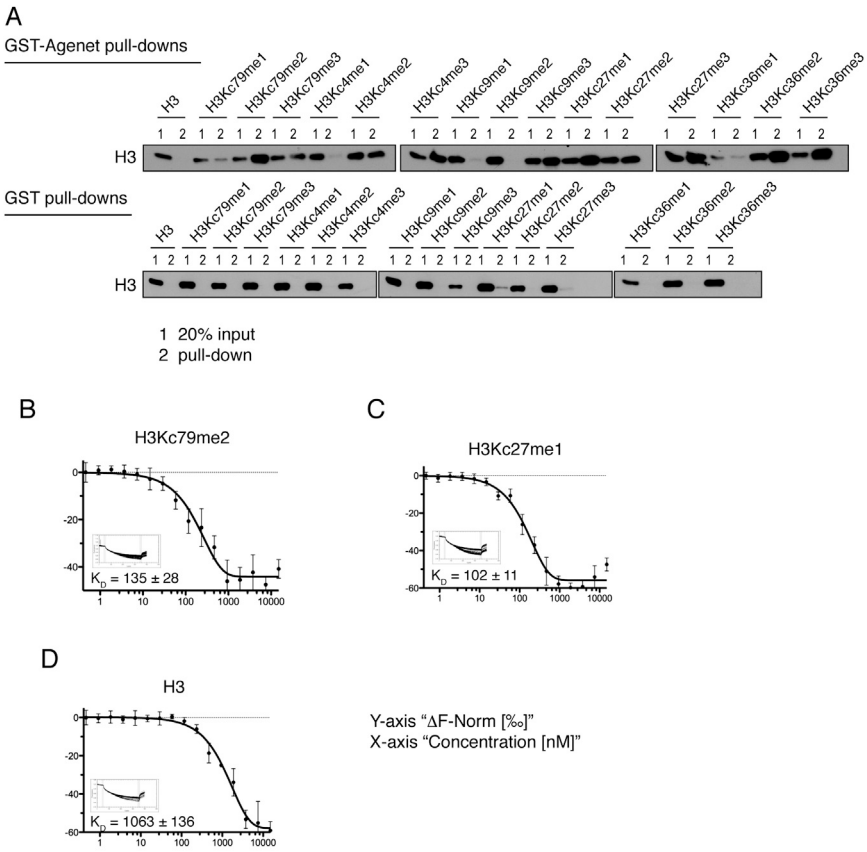

Figure S4. Agenet Domain Binding to Methylated MLA Histone Substrates, Related to Figure 3

(A) In vitro pull-downs using FMRP GST-Agenet domain and MLA histones carrying methyl lysine analogs at various sites.

(B–D) Equilibrium binding analysis of $Agenet_{FMRP}$ interaction with MLA histone substrates using microscale themophoresis (MST). Independent binding reactions were performed a minimum of three times. Data points were plotted with the x axis representing nM concentration of modified histone proteins and y axis representing ΔF_{Norm} [‰], which is the reduction of fluorescence due to directed movement of molecules in a microscopic temperature gradient.

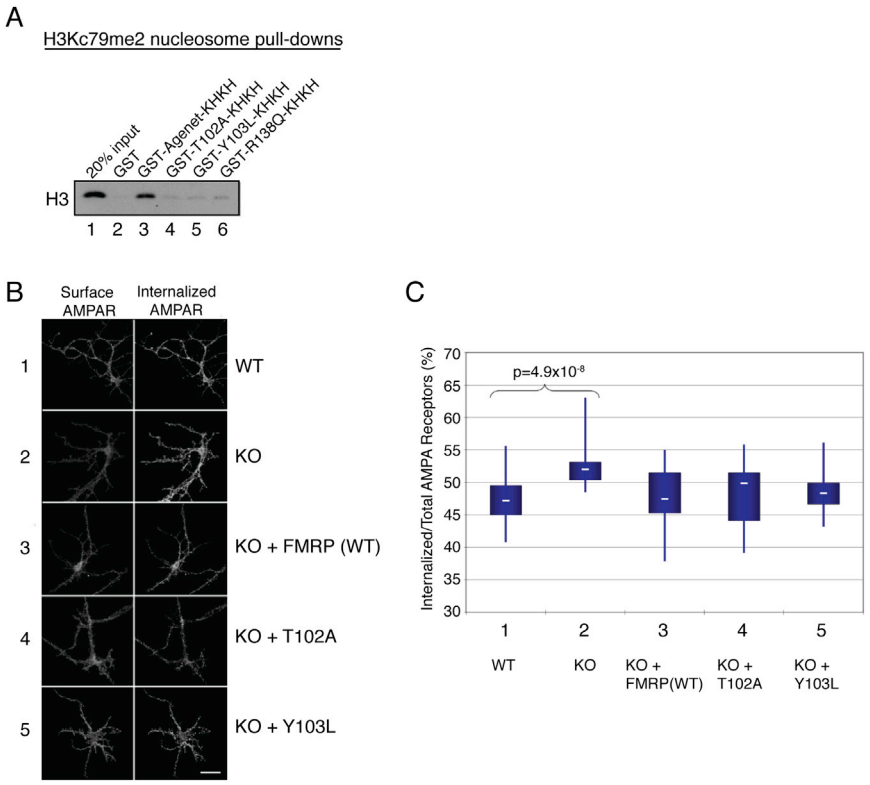

Figure S5. Genetic Complementation Experiments Using Wild-Type FMRP and Its Agenet Domain Mutants in the AMPAR Internalization Assay, Related to Figures 3 and 4

(A) In vitro H3K79me2 MLA nucleosome binding reactions using GST-AgenetKHKH domain. AgenetKHKH$_{FMRP}$ contains 2 additional nucleic acid binding domains adjacent to the double-tudor domain allowing nucleosomal binding. Wild-type FMRP bound H3Kc79me2, whereas Agenet domain mutants T102A, Y103L, and R138Q (patient mutant, see Figure S6A) did not (compare lanes 3 to 4,5, and 6).

(B) Hippocampal primary neurons from a wild-type and an *Fmr1* KO mouse, as well as neurons from *Fmr1* KO mouse reconstituted with lentiviral constructs expressing wild-type FMRP or FMRP mutants T102A and Y103L were immunostained for surface and internalized AMPARs. Internalized AMPAR signal was increased and AMPAR signal remaining on the surface was reduced in FMRP KO neurons as compared to wild-type neurons (panels 1 and 2). FMRP KO neurons infected with lentivirus expressing either wild-type or mutant forms of FMRP displayed reversal of the excessive AMPAR internalization observed in FMRP KO neurons (panels 3–5), indicating that Agenet mutations T102A and Y103L do not affect FMRP function at neuronal dendrites.

(C) Distribution of AMPARs in distal dendrites. Box-and-whisker plot showing that enhanced constitutive endocytosis of AMPARs in FMRP KO neurons (lane 2) is corrected by lentivirus expressing either WT (lane 3), T102A mutant (lane 4), or Y103L mutant (lane 5) FMRP. Median: WT, 47.18; KO, 52.01; KO+FMRP(WT), 47.44; KO+T102A, 49.86; KO+Y103L, 48.30; n = 30 each. p values were determined using one-way ANOVA (α = 0.05) with Bonferroni's post hoc test.

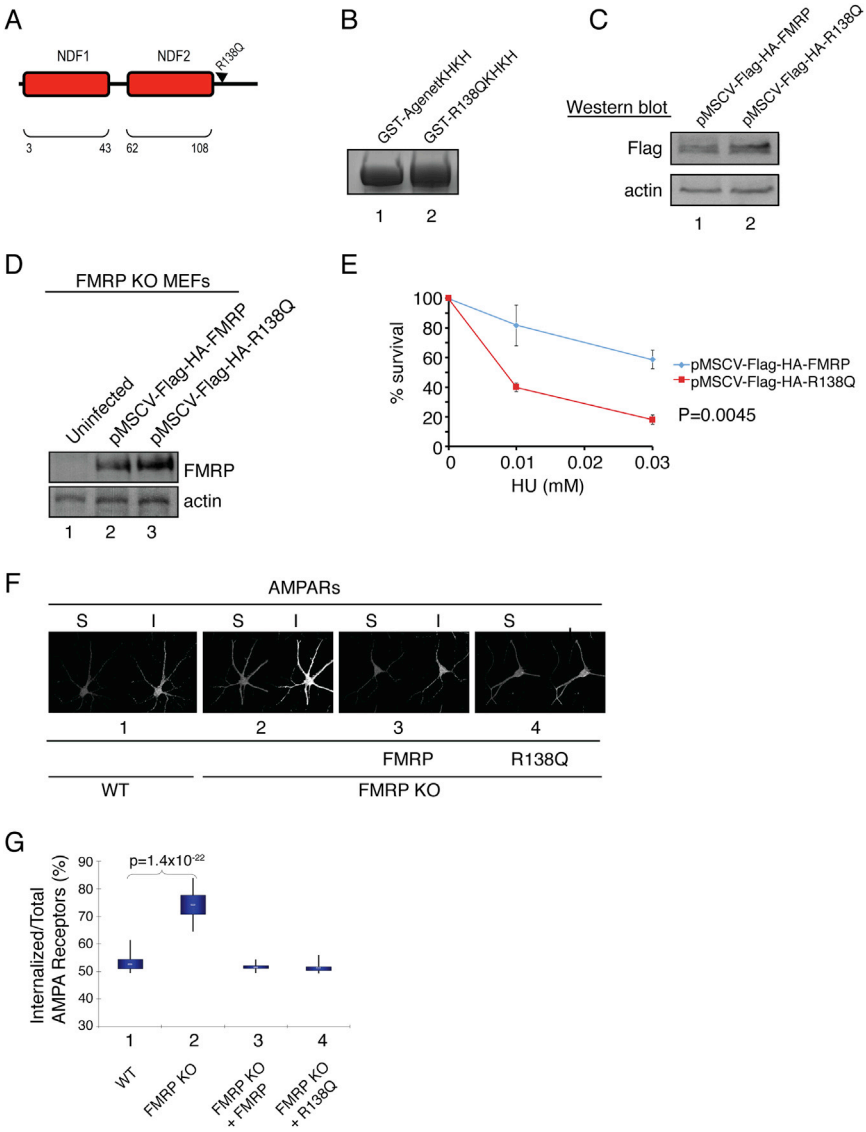

Figure S6. Analysis of the R138Q FMRP Patient Mutant in the Chromatin Interaction, DDR, and AMPAR Internalization Assays, Related to Figure 4

(A) Diagram of the FMRP Agenet double-tudor domain showing the location of the patient mutation R138Q.

(B) Coomassie gel showing GST-AgenetKHKH and GST-R138QKHKH proteins used in MST experiments for Kd determination.

(C) Western blot showing the levels of expression of exogenous Flag-HA-FMRP (lane 1) and FMRP (R138Q) Agenet domain patient mutant (lane 2) in FMRP KO MEFs, using anti-Flag antibody.

(D) Western blot showing the levels of expression of exogenous wild-type FMRP (lane 2) and R138Q FMRP patient mutant (lane 3) rescue constructs in FMRP KO MEFs using anti-FMRP antibody. Lane 1 contains FMRP KO MEFs without the rescue for comparison.

(E) Colony survival assay in the presence of hydroxyurea (HU) using FMRP KO MEFs reconstituted with wild-type FMRP or R138Q FMRP patient mutant. R138Q-reconstituted MEFs were more sensitive to the increased doses of HU as compared to wild-type FMRP reconstituted MEFs ($p = 0.0045$, 2-way ANOVA).

(F) Images of hippocampal neurons immunostained for surface (S) and internalized (I) AMPARs. Panel 1: wild-type neurons, panel 2: FMRP KO neurons, panel 3: FMRP KO neurons rescued with wild-type FMRP, panel 4: FMRP KO neurons rescued with FMRP R138Q mutant.

(G) Quantification of results in (F). Both rescue proteins functioned similarly in AMPARs internalization experiments, reversing AMPAR constitutive endocytosis in FMRP KO neurons. Compare lanes 3 and 4 (y axis is the ratio of internalized to total AMPARs). Median: WT, 52.60; KO, 74.20; KO+FMRP (WT), 51.57; KO+R138Q, 51.44; $n = 30$ each. p values were determined using one-way ANOVA ($\alpha = 0.05$) with Bonferroni's post hoc test.

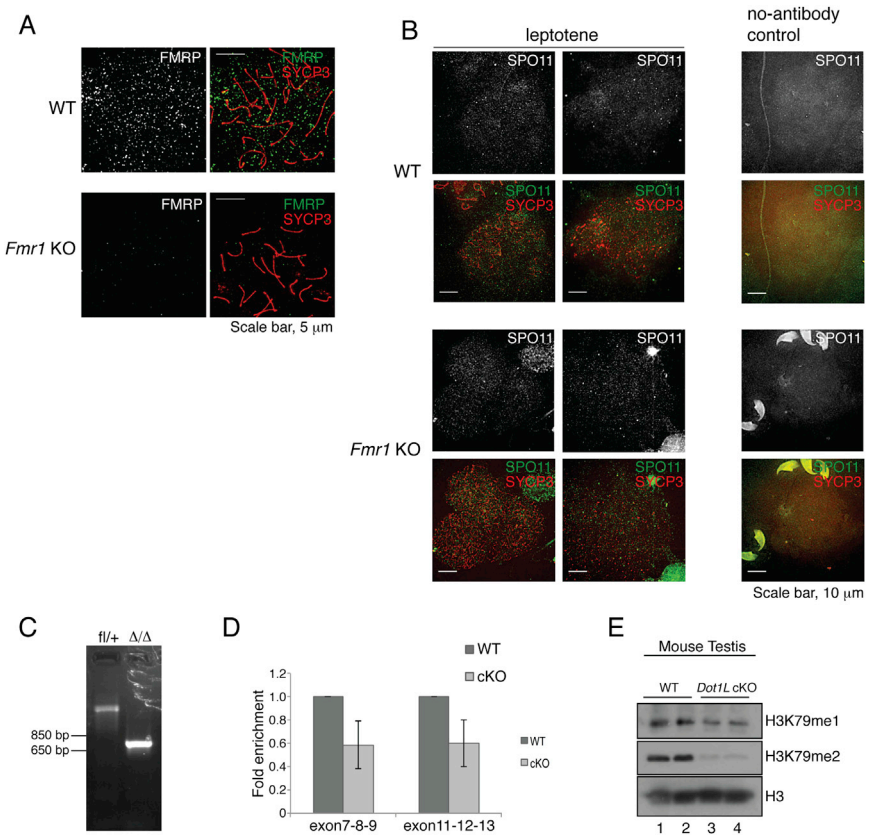

Figure S7. Control Staining of FMRP in Mouse Spermatocytes, SPO11 Staining, and Analysis of *Dot1L* cKO Testes, Related to Figures 5 and 7

(A) Immunostaining of wild-type (WT) and *Fmr1* KO meiotic spreads with anti-FMRP antibody (rabbit polyclonal anti-FMRP, Abcam) to confirm the specificity of FMRP staining. SYCP3 marks the chromosomes. Scale bar, 5 μm.

(B) SPO11 recruitment and double-strand-break formation is not perturbed in *Fmr1* KO cells. SPO11 catalyzes DSBs during the leptotene stage of meiotic prophase. Staining for SPO11 in representative WT and representative KO leptotene cells reveals no difference between WT and KO. Equivalent staining with no primary antibody is shown as a negative control. SPO11 staining alone is shown in the top row for clarity. Large green patches are sperm heads. Scale bar, 10 μm.

(C–E) *Dot1L* expression is reduced in *Dot1L* cKO testis.

(C) Genotyping for the $Dot1L^{\Delta}$ allele using genomic DNA from $Dot1L^{fl/+}$;*Mvh-Cre*- (WT, fl/+) or $Dot1L^{fl/\Delta}$;*Mvh-Cre*+ (cKO, Δ/Δ) adult testis tissue. The delta allele is predicted to be ~700 bp.

(D) qRT-PCR using two different primer sets specific for *Dot1L*, using cDNA from $Dot1L^{fl/+}$;*Mvh-Cre* (WT) and $Dot1L^{fl/\Delta}$;*Mvh-Cre*+ (cKO) adult testis. For each qPCR primer set, one primer spans an exon-exon junction in the *Dot1L* cDNA and the other primer is in a third, adjacent exon. Signal is normalized to *Actb*. Error bars signify SD for two biological replicates. Differences between means do not meet statistical significance. Note that cDNA was isolated from whole testis, which contains both somatic and germ cells, but the *Mvh-Cre* transgene is expressed only in germ cells. Therefore, some *Dot1L* expression is expected in the mixed somatic/germ cell population even in cKO testis.

(E) Western blot for H3K79me1 and H3K79me2 on mouse testis lysates showing reduction of H3K79 methylation in *Dot1L* cKO testes (lanes 3 and 4). Two samples of WT (lanes 1 and 2) and *Dot1L* cKO (lanes 3 and 4) testes are shown.